Field-scale evaluation of MN-sourced biochar for comprehensive contaminant removal from parking lot runoff

A Thesis

SUBMITTED TO THE FACULTY OF THE

UNIVERSITY OF MINNESOTA BY

Karina Weelborg

IN PARTIAL FULFILLMENT OF THE REQUIREMENTS

FOR THE DEGREE OF

MASTER OF SCIENCE

Dr. Joe Magner

Dr. Bridget Ulrich

March 2023

Acknowledgements

Support for this project is provided by the Stormwater Research and Technology Transfer Program with funding from the Clean Water Fund from the State of Minnesota's Clean Water, Land and Legacy Amendment. Additional support comes from the Minnesota Stormwater Research Council and its member cities, watersheds, private businesses, the University of Minnesota Water Resources Center, Minnesota Sea Grant, the College of Food, Agriculture, and Natural Resource Sciences, and the National Institutes for Water Resources funded by the US Geological Survey.

I would like to acknowledge and thank my advisors and committee members for their critical help and mentorship throughout the experiment and in the development of this thesis. We wish to acknowledge the contributions of all who helped make this work possible. Thank you to Tadele Haile, Brain Barry, Matt Young, and all other NRRI staff involved in preliminary experiments and the production and characterization of the biochar used in this thesis. Thank you to Jim Rudolph, Brian Jastram, and all other MWMO staff for helping to install, maintain, sample, and examine data from the MWMO filter testbeds.

Dedication

This thesis is dedicated to my husband, Dyllan, and my parents to whom I wish to express immeasurable gratitude. Without your unending love and support, this work would not have been possible. To God be the glory.

Abstract

The performance of catchment-scale filters containing sand and red-pine biochar, produced at 550^{o}C, were monitored for 2 years. Six events from the 2022 field season showed relative flow equalization between the sand and biochar filters and were used for detailed performance analysis. Both filters provided removal of *E. coli*, total phosphorus, metals, total organic carbon, and total suspended solids. The sand and biochar filters provided inconsistent removal of orthophosphate. Both filters exported nitrate, though the biochar filter to a lesser degree. The addition of biochar provided greater concentration decreases for zinc and total suspended solids though no statistically significant difference between the sand and biochar was found for any filter performance. Results from this study highlight the importance of adjusting biochar production conditions for development of characteristics needed for contaminant removal and the importance of validating laboratory results in the field.

Table of Contents

Table of Figures

Table of Tables

1. Introduction

1.1 Urban Stormwater Pollution

Stormwater, defined as any water that runs over the land's surface after a rain or snowmelt event, has been described as "one of the greatest challenges of modern water pollution control" partly due to the complex mixture of contaminants it carries to receiving waters (MN SSC 2008; NRC and NAP 2009). As populations and urban centers continue to grow, water scarcity across the United States becomes an ever-increasing problem, making protection of these freshwater sources even more important (Grebel et al. 2013). Simultaneously, the threat of resource degradation is likely to increase with increasing urbanization and changing climactic patterns (US EPA 2016; Hettiarachchi et al. 2018).

The state of Minnesota has bountiful water resources, including nearly 70,000 miles of water courses, 9 million acres of wetlands, and thousands of miles of trout streams in addition to the many more than the 10,000 lakes that earn the state its nickname, the "Land of 10,000 Lakes" (MN SSC 2008). Water resources are an engrained part of Minnesota's cultural identity, and as such, protection of the state's irreplaceable resources is a necessity. Contaminants, taken up by stormwater from urban and residential surfaces, are transported to receiving waters leading to degraded aquatic habitats, compromised recreational activities, and increased treatment costs at water treatment plants (Grebel et al. 2013). A 2002 assessment of Minnesota waters found that nearly 45% of streams and rivers and 47% of lakes did not meet state water quality standards (NRC and NAP 2009).

Stormwater is of particular concern in urban centers as urban runoff is largely responsible for the impairment of over 68,000 miles of rivers and streams and 948,000 acres of lakes in Minnesota (NRC and NAP 2009). Urban centers account for substantial volumes of stormwater runoff due to changes in the face of the landscape, particularly by impervious surfaces that alter natural hydrologic conditions and geomorphology (MN SSC 2008; Grebel et al. 2013). Soil compaction and built impervious surfaces lead to increased runoff and peak discharge volumes by decreasing infiltration and ultimately redirecting

runoff to receiving waters. Anthropogenic drainage systems within the urban environment also increase runoff velocities. These hydrologic concerns increase the frequency and intensity of flooding events. While these flooding events have conventionally been the reason for stormwater management in urban areas, water quality is also a concern. Urban activities increase pollutant quantities, and impervious surfaces increase the volume and rate at which pollutants enter receiving waters (MN SSC 2008; Grebel et al. 2013; Mohanty and Boehm 2014; Ulrich et al. 2015).

Stormwater can contain complex mixtures of physical, chemical, and biological contaminants. Sediments in stormwater are of particular concern as fine sediments can bind pollutants and transport them downstream (Sansalone and Kim 2008). Other contaminants commonly found in stormwater include *E. coli*, nutrients, metals and organics (MN SSC 2008; Grebel et al. 2013; Mohanty et al. 2018). These contaminants are commonly sourced from erosion, fertilizer and pesticides, yard waste, leaking sewer lines, industrial air pollution, vehicular use, and municipal maintenance activities.

The removal of pollutants from stormwater is essential as they can cause a variety of concerns in the natural and urban environment. The presence of *E. coli* has been responsible for disease and beach closures. However, its removal from stormwater is difficult as it can use nutrients in stormwater for growth and can be mobilized during stormwater's intermittent flows (NRC and NAP 2009; Mohanty et al. 2018). Nutrients in stormwater include nitrogen and phosphorus species which can cause excessive algal growth, eutrophication, and fish kills (MN SSC 2008). Heavy metals often found in stormwater include chromium, copper, nickel, lead, and zinc. These metals are nonbiodegradable, highly toxic at low concentrations, and have stormwater concentrations that are greater than aquatic organism thresholds (Liu and Zhang 2009; Grebel et al. 2013; Mohanty et al. 2018). Organic contaminants are toxic to surface waters and can be carcinogenic (MN SSC 2008; Ulrich et al. 2017; Mohanty et al. 2018; Boehm et al. 2020).

1.2 Stormwater Best Management Practices

Low impact development (LID) has gained traction as a means for stormwater volume control within urban centers (NRC and NAP 2009; Mohanty et al. 2018). The primary purpose of LID systems has traditionally been flood control with pollutant removal considered a secondary objective (MN SSC 2008; NRC and NAP 2009; Boehm et al. 2020). Typical LID best management practices include biofiltration basins, retention basins, sand filters, porous pavement, and dry/wet ponds (MN SSC 2008; Grebel et al. 2013; Mohanty et al. 2018).

Filtration systems can be designed with a focus on water quality improvements. These improvements can be achieved by selecting filter media to remove specific contaminants. Conventional filtration media mixtures include sand, gravel, and native soils (Grebel et al. 2013; Boehm et al. 2020). Approximately 70-85% of conventional filtration media is medium to course sand (Mohanty et al. 2018). Course media allows high hydraulic conductivity and effective removal of sediment and particulate-bound pollutants such as metals and hydrophobic organic contaminants like polyaromatic hydrocarbons (Grebel et al. 2013; Ulrich et al. 2017; Mohanty et al. 2018; Boehm et al. 2020). The primary mechanism of removal in sand filters is mechanical filtration with limited sorption, ion exchange, electrostatic and hydrophobic interactions, and other chemical processes (Hatt et al. 2007; Ulrich et al. 2017; Mohanty et al. 2018; Boehm et al. 2020; Ekanayake et al. 2021). The use of filtration media with particle distributions that match the distributions found in sediments can increase contaminant removal performance of sand filters (Hatt et al. 2007). However, the pollutant removal capacity of sand filters for dissolved contaminants remains low with variable removal and even export of nutrients, microbial contaminants, and trace organic contaminants (Grebel et al. 2013; Payne et al. 2014; Ulrich et al. 2017; Mohanty et al. 2018; Boehm et al. 2020; Erickson et al. 2021; Tirpak et al. 2021).

1.3 Biochar as a Filter Media Amendment

Enhancement of filtration media is key to improve contaminant removal. Sand media's low capacity for dissolved contaminants is due to several factors including a lack of internal pore space, low water retention capacity for recovery after drying periods, and low cation exchange capacity (Hatt et al. 2007; Grebel et al. 2013; Payne et al. 2014). Conventional sand media can be augmented with filter media amendments to enhance contaminant removal and improve the overall performance of filtration systems. Amendments rich with calcium oxide, with high cation exchange capacities, and with metal oxides respectively promote contaminant precipitation, ion exchange, and chemisorption (Grebel et al. 2013). To be truly effective, geomedia amendments must not only provide effective pollutant removal under variable conditions but also mitigate flooding (i.e., high hydraulic performance) and be available at low cost.

1.3.1 Biochar production and properties

Biochar is a low-cost, solid, carbonaceous material produced via thermal decomposition of biomass. Biochar has long been used as a soil amendment due to unique properties that increase nutrient availability, microbial activity, organic matter content, and water retention (Mohan et al. 2014). Properties of biochar that increase important soil qualities, such as surface area, ion exchange capacity, and interparticle porosity, vary greatly according to biochar production conditions and feedstock type. While the extent of these properties is not critical for soil amendment, specific biochar properties are required to effectively improve filter pollutant removal capacity. Fortunately, biochar properties are tunable according to production conditions and feedstock type. This tunability provides an opportunity to select conditions to produce materials that target specific pollutants.

Biochar is conventionally produced via pyrolysis, which involves the thermal decomposition of organic matter under low oxygen conditions. Pyrolysis can be completed in a batch or continuous fashion over a wide range of temperatures, at low or high heating rates, and for short or long residence times with each parameter promoting different biochar characteristics (Liu et al. 2015; Qian et al. 2015; Panwar et al. 2019;

Yaashikaa et al. 2020; Veiga et al. 2021). Fast pyrolysis processes are typically characterized by high heating rates and short residence times ranging from seconds to minutes while slow pyrolysis is characterized by lowered heating rates and longer residence times ranging from minutes to hours (Liu et al. 2015; Qian et al. 2015; Yaashikaa et al. 2020). Batch production of biochar produces small batches of biochar at a lowered cost, but consistency between batches is difficult to maintain (Panwar et al. 2019; Veiga et al. 2021). As such, batch production is most suited to small scale lab experiments. In contrast, a continuous production of biochar is much more suited for commercial production and large scale experiments, as higher yields, greater consistency, and larger quantities of biochar can be produced (Panwar et al. 2019; Veiga et al. 2021).

Pyrolysis can be conducted from low temperatures near 250^{o}C to very high temperatures greater than 800^{o}C. Lower pyrolysis temperatures (i.e., less than 500 °C) result in greater biochar yields but lower surface area, pore volume, and pH; and are associated with stronger negative charges, higher cation exchange capacities, and greater quantities of hydrophilic functional groups (Streuble 2015; Ulrich et al. 2017; Mohanty et al. 2018). These lower temperature biochars can also contain residual labile organic matter, which is toxic to aquatic organisms (Hale et al. 2012). Higher temperature pyrolysis can be used to avoid this toxicity as further degradation of the biomass occurs (Veiga et al. 2021). Higher pyrolysis temperatures produce lower yields of biochars that have greater surface area and intraparticle surface area, higher ash content and pH, and more hydrophobic aromatic surface character. Feedstock material also determines biochar properties as biochar retains the pore structure of its feedstock (Mohanty et al. 2018). Biochars produced from softwoods tend to have higher surface area than those produced from hardwoods due to a decreased density that leaves the wood prone to greater thermal decomposition (Mohanty et al. 2018).

1.3.2 Contaminant Removal Mechanisms of Biochar

Amendment of sand with biochar has been shown to increase straining capabilities, water retention, and permeability, leading to more resilient pollutant removal, particularly during intermittent flows inherent to stormwater (Grebel et al. 2013; Barnes et al. 2014;

Mohanty et al. 2018). Lower temperature biochars have been shown most effective for the removal of suspended solids and metals due in large part to their high cation exchange capacities and hydrophilic functional groups (Uchimiya et al. 2011; Gwenzi et al. 2017; Ulrich et al. 2017; Mohanty et al. 2018). Higher temperature biochars retain removal of metals and sediments while showing greater potential for neutral and hydrophobic organic contaminants due to greater quantities hydrophobic aromatic surface character (Grebel et al. 2013; Mohan et al. 2014; Ulrich et al. 2017; Mohanty et al. 2018; Saiz-Rubio et al. 2019). Removal of dissolved nutrients and bacteria remains inconsistent regardless of pyrolysis temperature (Ulrich et al. 2017; Mohanty et al. 2018; Erickson et al. 2021).

Conventional filtration media removes *E. coli* via straining, inactivation, microbial predation, and die off (Zhang et al. 2010; Grebel et al. 2013; Mohanty and Boehm 2014; Mohanty et al. 2018). Biochar has been shown to enhance *E. coli* removal by facilitating adsorption via hydrophobic and steric interactions (Mohanty and Boehm 2014). As higher pyrolysis temperatures lead to more aromatic and hydrophobic surface character, application of a high temperature biochar is critical to enhance *E. coli* removal relative to conventional sand mixtures (Mohanty and Boehm 2014; Valenca et al. 2021). Biochars have also been shown to reduce remobilization of *E. coli* during intermittent flow due to greater water retention capacity and the potential for stronger binding (Mohanty et al. 2014; Mohanty and Boehm 2014; Mohanty et al. 2018).

Removal of nitrate and phosphorus species is often difficult to obtain in a single system as the anoxic conditions required for denitrification can lead to leaching of iron-sorbed phosphate (Grebel et al. 2013; Mohanty et al. 2018; Fischer and Feinberg 2019). While the use of biochar to remove phosphorus from stormwater has produced mixed results (Erickson et al. 2021; Chen et al. 2022), several studies have shown promise for biochar to enhance nitrate removal (Payne et al. 2014; Ulrich et al. 2017; Tian et al. 2019; Chen et al. 2022). Nitrate removal is highly variable in filtration systems, and studies evaluating the effects of biochar on nitrate removal have shown mixed results (Payne et al. 2014). Denitrification requires anaerobic conditions not always present in traditional filtration systems (Payne et al. 2014; Bock et al. 2015). Biochar amendment can improve

water retention relative to conventional media, promoting the development of a micro-anoxic environment in capillary water (Chen et al. 2022). Conditions such as these are favorable to the formation of microbial communities of heterotrophic bacteria that promote denitrification (Bock et al. 2015; Mohanty et al. 2018). Biochar can also serve as an electron donor for denitrifying bacteria, which also may contribute to observations of enhanced denitrification (Tian et al., 2019).

Metals are present in stormwater in either the dissolved or particulate-bound phase. Metals can be removed via straining of bound particles, complexation, cation exchange, electrostatic interactions, precipitation, and chemical reduction dependent on the specific metal contaminant (Liu and Zhang 2009; Mohanty et al. 2018; Boehm et al. 2020). Most studies show a consistently high removal of heavy metals like copper, lead, and zinc (Mohanty et al. 2018; Gwenzi et al. 2017). Dissolved heavy metals are primarily removed through sorption processes. Ion exchange is an important removal mechanism for dissolved species with exchanges occurring with cations such as sodium, potassium, calcium, and magnesium (Li et al. 2017; Mahdi et al. 2018). Electrostatic interactions between metals and media is heavily dependent on solution pH with metal removal increasing with increasing pH (Kołodyńska et al. 2012; Mahdi et al. 2018).

1.5 Field-Scale Evaluation of Biochar-amended Filtration Systems

While laboratory and bench-scale studies have shown promise for biochar's effectiveness as a stormwater filtration amendment, studies evaluating the application of biochar-amended filtration systems are limited and have variable results. The differences in performance are due largely to varying biochar properties and limited research at the field-scale under environmentally realistic conditions. Laboratory studies often use a limited number of contaminants in influent and do not accurately represent the complex mixtures seen in urban stormwater. Similarly, field aging from stormwater creates greater competition for attachment sites and freeze-thaw cycles create preferential flow that can potentially decrease removal capacity (Mohanty et al. 2014; Mohanty et al. 2018; Boehm et al. 2020; Chen et al. 2022). Field-scale experiments under these complex conditions

can inform on the applicability of lab scale experiments and will assist in furthering widespread application of biochar as a media amendment.

1.5.1 Objectives

This research aims to characterize comprehensive contaminant removal of biochar-augmented stormwater filters at the catchment scale to provide a better understanding of the applicability of biochar in the field. To achieve this goal the following objectives were made: (1) produce a Minnesota sourced and produced biochar that can provide effective comprehensive contaminant removal and (2) analyze the biochar-augmented media's performance in field scale testbeds over 2 years. Objective 1 was completed in 2020 and 2021 at the Natural Resources Research Institute (NRRI). At NRRI, bench scale experiments were completed for 14 biochars produced at different pyrolysis temperatures and from differing feedstocks. According to results from these experiments and large-scale production limitations, a red pine biochar produced at 550^{o}C was chosen for field-scale experiments. To accomplish objective 2, the red pine biochar was deployed in May 2021 at the Mississippi Watershed Management Organization (MWMO). Three filter testbeds were filled with biochar-augmented sand, a control sand, and iron-enhanced sand media for comparison. Analysis of filter performances is presented below.

2. Materials and Methods

2.1 Filter Materials

2.1.1 Sand Materials

C33 fine aggregate washed concrete sand (0.0% gravel, 99.3% sand, and 0.7% silt and clay) was purchased from Plaisted Companies in Elk River, MN. Iron enhanced sand was also purchased from Plaisted Companies and consists of washed concrete sand combined with Connelly-GPM iron aggregate at 5.6%. Particle size distribution for the concrete sand is listed in Table 1.

Table 1. Concrete Sand Particle Size Distribution
Particle size distribution information was provided by Plaisted Companies.

Sieve Size	Passing (%)
9.5 mm (3/8 inch)	100
4.75 mm (No. 4)	100
2.36 mm (No. 8)	96
1.18 mm (No. 16)	83
600 um (No. 30)	60
300 um (No. 50)	23
150 um (No. 100)	4
75 um (No. 200)	0.7

2.1.2 Biochar Material

Red pine wood chips were used as biochar feedstock. This feedstock was selected based on preliminary batch screening tests that evaluated the sorption of dissolved organic carbon and removal or release of phosphorus. Results of the preliminary batch screening tests showed that biochar produced from the red pine wood chips did not release phosphate and was able to achieve DOC removal similar to that of a high temperature commercial biochar.

Biochar production occurred in the rotary kiln at the NRRI Colerain Biomass Conversion Lab. As-received wood chips were screened to between 4.76 mm and 19.0 mm and dried to an approximate moisture content of 5 to 15%. The dried woodchips were fed to a rotary kiln at a feed rate of ~0.9 kg to 1.8 kg per minute. and pyrolyzed at a constant pyrolysis temperature of 550^{o}C with a residence time of 15 minutes. Production occurred on March 25th, March 30th, and March 31st in 2021. Following pyrolysis biochar was placed in Surge Bin agitators until the majority of particles were smaller than 3.36 mm. Particles were then sieved to between 0.55 mm and 3.36 mm. Final particle size distribution is shown in Table 2. An approximate 22% dry yield of biochar was achieved.

Table 2. Final Biochar Screen Yields

	Wet Yield at ~ 3% Moisture (kg)	Dry Yield (kg)
>3.36 mm	7.71	7.48
0.500 mm – 3.36 mm	131.99	128.03
< 0.500 mm	39.01	37.84

2.2 Site description

The field site is located at the MWMO Stormwater Park and Learning Center in Minneapolis, MN. Precipitation is measured by an automated rain gauge onsite, and the catchment area is 0.41 acres (Figure 1). The system consists of a basin with 3 separate filter testbeds (Figure 2). The basin receives runoff from a parking lot shared by MWMO and the neighboring bar, Tony Jaros River Gardens. Runoff is collected in a catch basin for settling pretreatment and is then conveyed to a weir box that discharges to the 3 testbeds that are 20.25 ft (sand) or 21.25 ft (biochar, IES) in length. Testbeds are constructed from 4 ft diameter corrugated polyethylene pipe half-sections, with a 4 in drain tile at the bottom. Runoff exits the system via the drain tile into an effluent weir box for each filter (Figure 3). A HOBO water level logger and pressure transducer were placed on the bottom of the parking lot weir box and each effluent weir box.

Fresh filter media was installed in the testbeds in May 2021. The three testbeds were filled with either biochar-amended sand, sand, or IES. Biochar and sand were mixed onsite using an electric cement mixer (20 vol% biochar in sand, Figure 4). Sand and IES were installed in the testbeds as received. During installation, media were raked as the testbeds were filled to achieve uniform distribution (Figure 5).

Because influent parking lot discharge was not evenly distributed between the three filter testbeds, bricks were placed on the apron directing flow to the filter testbeds. Bricks can be seen in Figure 2. Several configurations of bricks were used throughout 2021 and 2022 until the majority of flow was directed to the sand and biochar filter testbeds.

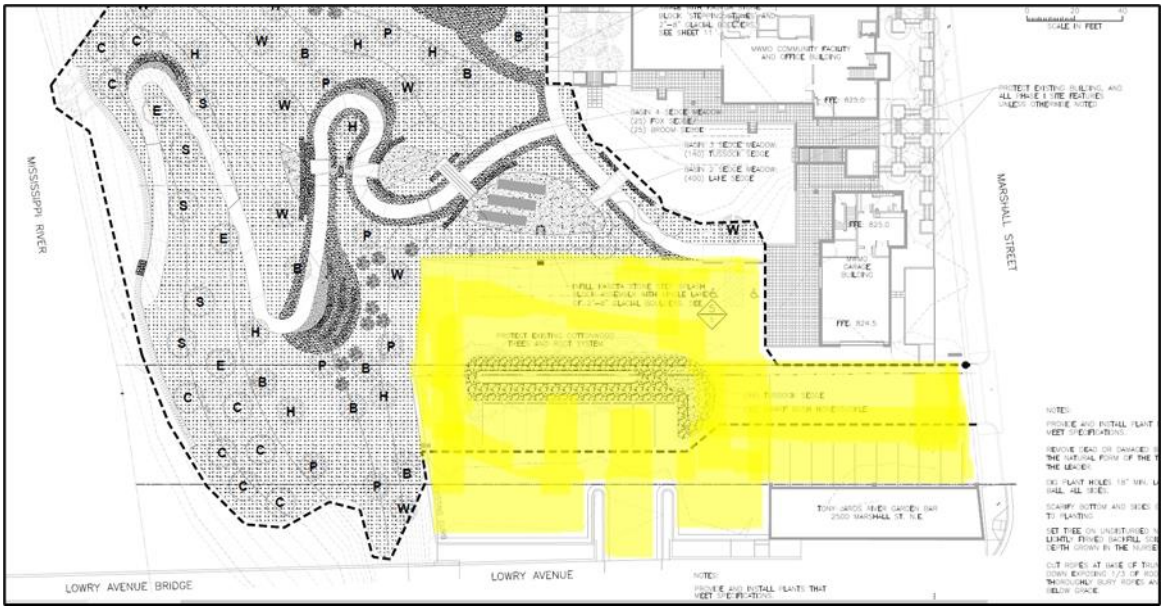

Figure 1. MWMO Field Site Catchment Area
Taken from the MWMO 2011 Landscape Plan. The system catchment area is highlighted.

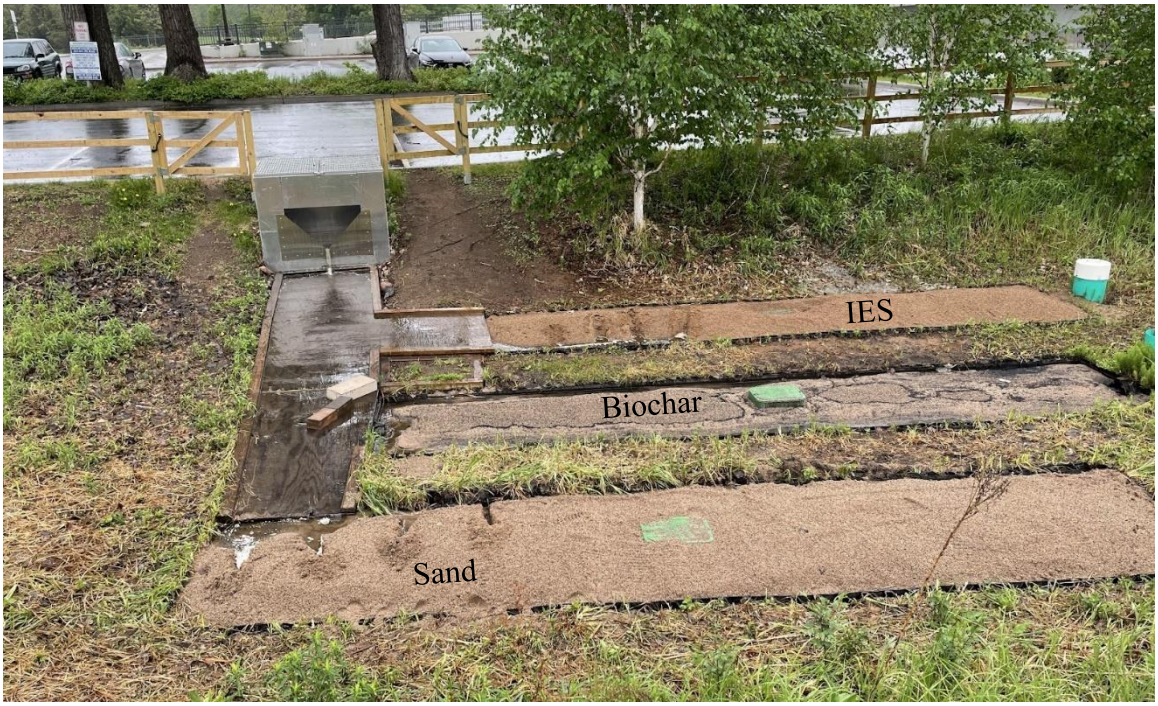

Figure 2. MWMO Filter Testbeds
Pictured here are the MWMO filter testbeds and parking lot weir box. The parking lot weir box collects parking lot runoff and discharges flow to an apron that distributes flow to the testbeds. As flow was not evenly distributed, bricks were used to direct flow towards the biochar and sand filters. Pictured here is an early brick configuration from 2021.

Figure 3. Effluent Weir Boxes for Filter Testbeds
Pictured here are the effluent weir boxes of the filter testbeds during a sampling event with sample bottles placed atop their respective weir box.

Figure 4. Using a Cement Mixer for Biochar and Sand Mixing
Pictured here is John Mueller, formerly of MWMO, emptying mixed sand and biochar from the cement mixer into a wheelbarrow for transport to the testbed.

Figure 5. Raking the Biochar Filter
Pictured here are Dr. Udai Singh, MWMO, and Dr. Tadele Haile, NRRI, raking media.

2.3 Performance monitoring

Grab samples were collected approximately twice per month from spring to fall over 2021 and 2022. Fourteen samples were taken in 2021, and 12 samples were taken in 2022. Qualifying storms were determined as defined in the EPA Industrial stormwater monitoring and sampling guide (EPA 2009). Briefly, samples were collected for events that (1) caused measurable discharge from both the influent and effluent basin, (2) occurred at least 72 hours after the previous qualifying event, and (3) occurred from sunrise to an hour before sunset. Some samples were taken outside of these parameters to ensure adequate sampling size.

Whirlpaks were used for collection of *E. coli* samples. Grab samples for water quality analyses were collected in four-liter bottles provided by the Metropolitan Council Environmental Services (MCES) laboratory. Samples were collected from each of the four weir boxes (the influent weir box discharging from the parking lot and the effluent weir boxes at the outlet of the three testbeds) from the center of flow without pre-rinsing or overfilling. Immediately following collection, a YSI ProDDS multiparameter sonde

was used to measure temperature, dissolved oxygen, conductivity, salinity, and pH. Transparency measurements were then taken from influent and effluent weir box flows using a secchi tube. Samples were refrigerated prior to transport to MCES labs for analysis. After each sampling event, the MWMO Site Rain Sampling Google form was completed to document site, station, date and time, sampling personnel, sonde measurements, and visual assessment of samples.

Samples of the filter media were collected at the end of each sampling season for measurement of moisture content, porosity, and bulk density. Three 10-inch cores and 2 3-inch cores were taken from along the length of each testbed with shallow cores between the deep cores. Hydraulic conductivity was measured using an automated Modified Philip-Dunne (MPD) Infiltrometer from Upstream Technologies according to manufacturer recommended procedures. Hydraulic conductivity was measured once after each field season. In 2021, 2 measurements were taken along the length of each filter. In 2022, 3 measurements were taken along the length of each filter.

Samples for analysis of trace organic contaminants were collected as grab samples approximately once a month. Samples were filled in the same manner as general water samples but were only taken from parking lot influent and sand and biochar effluent weir boxes due to budget constraints. Samples were collected in methanol-rinsed 120-mL amber glass jars and were frozen prior to transport to NRRI for analysis. Analysis of these samples is currently pending and will be provided in the final project report.

2.3 Flow Monitoring

Water levels were continuously collected at five-minute intervals at the four weir boxes and converted to discharge using the Cone equation (Equation 1) as recommended by the Bureau of Reclamation Water Measurement Manual (USBR 2001).

$$Q = 2.49*H^{2.48} \qquad \text{Equation 1}$$

Q is discharge over the weir in cubic feet per second, and H is head over the weir in feet. H was calculated by subtracting the weir crest height from the recorded water level. As level loggers were placed on the bottom of weir boxes, the sensor depth was used as the

water level. Discharge data was converted to the appropriate metric units. Loggers were installed in early May 2021 and removed before freezing conditions. Loggers were reinstalled in the effluent weir boxes in early April 2022 and in the parking lot weir box in early May 2022.

Analysis of the 2021 flow data revealed discrepancies in flow measurements that have prevented proper interpretation of performance data from the first year of operation (Appendix, Hydrologic Characterization). Briefly, the cumulative outflow from the three filter boxes exceeded the cumulative inflow measured at the influent weir box by nearly double. Further inspection of monthly cumulative volumes and comparison with total volumes calculated from precipitation depths suggested the discrepancy was due to an error in the pressure measurements from the sensor located in the biochar testbed. MWMO is currently investigating the issue to determine if the flow data can be corrected retroactively. In light of these uncertainties, the analyses and discussions herein will be focused on data collected during the 2022 field season, for which we did not observe the same discrepancies. As the testbeds were likely undergoing equilibration due to compaction and biological augmentation during 2021, we expect that the data for the 2022 field season will be more representative of long-term performance. A complete summary of the 2021 flow and water quality data for 2021 is presented in the Appendix, to be interpreted with discretion pending a resolution to the flow data discrepancy by MWMO.

2.5 Analytical Methods

2.5.1 Biochar Characterization

Physicochemical properties of two biochars (the red pine biochar produced at NRRI and a commercial biochar obtained from American Biochar Company, Niles, MI) were determined through various characterization techniques. Proximate (ash content, volatile matter, fixed carbon, and sulfur content) and ultimate (carbon, hydrogen, nitrogen, and oxygen content) analysis was performed following corresponding ASTM Standard methods listed in Table 3. Pore size distributions (PSDs) of the biochar sample were

generated by combining results from nitrogen adsorption, carbon dioxide adsorption, and mercury intrusion porosimetry experiments.

Table 3. Biochar Characterization Analysis Methods

Parameter	Method
Moisture total (wt%)	ASTM E871
Ash (wt%)	ASTM D1102
Volatile matter (wt%)	ASTM D3175
Fixed carbon by difference (wt%)	ASTM D3172
Sulfur (wt%)	ASTM D4239
SO_2 (lb/mmbtu)	Calculated
Gross Cal. Value at Const. vol. (btu/lb)	ASTM E711
Carbon (C) (wt%)	ASTM D5373
Hydrogen (H) (wt%)	ASTM D5373
Nitrogen (N) (wt%)	ASTM D5373
Oxygen (O) (wt%)	ASTM D3176

To generate a continuous, complete pore size distribution (PSD, 0.36 to 325,000 nm), data from carbon dioxide adsorption isotherms, nitrogen adsorption isotherms, and mercury intrusion porosimetry were combined. For data corresponding to pore diameters in the range of 0.36 to 26.5 nm, a dual gas analysis previously published was followed (Jagiello et. al. 2013). Briefly, isotherm data from both carbon dioxide (273 K) and nitrogen (77 K) adsorption experiments were collected using a Micromeritics 3Flex instrument on biochar samples which had been degassed in vacuo at 250°C for 15 hours. The resulting data sets were simultaneously fit using a 2D non-local density functional model where the carbon surface was treated as heterogenous. For data corresponding to pore diameters from >26.5 nm to 325,000 nm (corresponding to applied pressures of ~0.55 to 6,800 psia), mercury intrusion porosimetry data was collected on a Micromeritics AutoporeV instrument. Once combined, a continuous data set for both incremental and cumulative pore volumes vs. pore diameter was generated allowing users to easily determine total pore volumes within the user-defined range. It should be noted that, while mercury intrusion porosimetry experiments collected data for pore widths all

the way up to 325,000 nm, intrusion >50,000 nm is due to interparticle pores, not particle pores.

Biochar's pH was measured using a biochar-to-water mass ratio of 1:5 followed by a 24 hour equilibration period (Li et al. 2013). The pH of the slurry was measured using a pH electrode (Fisher Brand Accumet AB150).

2.5.2 Water Quality Analysis

Water samples were sent to MCES labs for analysis of barium, chloride, *E. coli*, hardness, cadmium, chromium, copper, lead, nickel, zinc, ammonia nitrogen, nitrate, nitrite, total Kjeldahl nitrogen, total phosphorus (TP), orthophosphate (OrthoP), titanium, total organic carbon (TOC), total suspended solids, (TSS) and volatile suspended solids. The analytical methods performed by MCES are listed in Table 4.

2.5.3 Filter Properties

The bulk density of the media cores was calculated by dividing sample weight by core volume. To calculate moisture content, cores were microwaved in 4-min increments until weight stabilized. Post-microwaved weight was subtracted from pre-microwaved weight and divided by pre-microwaved weight for g/g moisture content. To calculate porosity, a graduated cylinder was filled with media to a marked level and weighed. Water was poured into the cylinder to the marked level, volume added recorded, and then weighted. The porosity was then calculated as the volume of water added divided by the total volume multiplied by 100%. The automated MPD-infiltrometer calculated saturated hydraulic conductivity using ASTM Standard D8152. Filter property data is available in the Appendix, Media Characterization.

Table 4. MCES Analysis Methods

Analyte (units)	Method Reference	Method Detection Limit
Barium (ug/L)	EPA 200.8, Rev. 5.4	0.08
Chloride ion (mg/L)	SM 4500-CL- E-2011	0.5
E. coli (MPN/100 ml)	SM 9223 B (Colilert-18 w/ Quanti-Tray)-04	N/A
Hardness (mg/L_CaCO3)	EPA 130.1	8
Cadmium (ug/L)	EPA 200.8, Rev. 5.4	0.2
Chromium (ug/L)	EPA 200.8, Rev. 5.4	0.08
Copper (ug/L)	EPA 200.8, Rev. 5.4	0.3
Lead (ug/L)	EPA 200.8, Rev. 5.4	0.1
Nickel (ug/L)	EPA 200.8, Rev. 5.4	0.3
Zinc (ug/L)	EPA 200.8, Rev. 5.4	0.8
Ammonia Nitrogen (mg/L)	EPA 350.1, Rev. 2.0	0.02
Nitrate N (mg/L)	SM 4500-NO3- F-2011	N/A (calc)
Nitrite N (mg/L)	SM 4500-NO3- F-2011	0.007
Nitrite Plus Nitrate (mg/L)	SM 4500-NO3- F-2011	0.02
Total Kjeldahl Nitrogen (mg/L)	EPA 351.2, Rev. 2.0	0.03
Total Phosphorus (mg/L)	EPA 365.4	0.02
Ortho Phosphate as P (mg/L)	SM 4500 P-F-2011	0.005
Titanium (ug/L)	EPA 200.8, Rev. 5.4	0.2
Total Organic Carbon (mg/L)	SM 5310 C-2011	0.05
Total suspended solids (mg/L)	SM 2540 E-2011	1
Volatile suspended solids (mg/L)	SM 2540 E-2011	1

2.6 Data analysis

Flow distribution between filters was calculated according to equation 2.

$$\frac{\text{Summation of outflow at time of sampling}}{\text{Filter Outlfow at Time of Sampling}} * 100\% \qquad \text{Equation 2}$$

To ensure that comparisons between conditions were interpreted for equivalent conditions, we focused our analysis on events where flow equalization was achieved within 25%. As the flow directing bricks were arranged by MWMO staff to direct the flow away from the IES filter, our analyses were restricted to six events where flow equalization was achieved between the biochar and sand testbeds (Table 6). For each flow-equalized event, event measured influent and effluent volumes were calculated by isolating events within the flow data. The 5-minute averages were multiplied by 300 seconds, summed for each event, and converted to the appropriate metric unit. The pore volume of each test bed and the number of pore volumes per event were calculated according to equations 3 and 4 respectively.

$$\text{Pore Volume} = \text{Testbed Volume} * \text{Measured Media Porosity} \qquad \text{Equation 3}$$

$$\text{\# of Pore Volumes} = \frac{\text{Event Influent Discharge}}{\text{Testbed Pore Volume}} \qquad \text{Equation 4}$$

The percentage of precipitation that resulted in outflow was calculated according to equation 5.

$$\frac{\text{Total Event Outflow}}{\text{Precipitation Volume}} = \frac{\Sigma(\text{Outflow Volume at Time of Sampling})}{\text{Precipitation Volume}} * 100\% \qquad \text{Equation 5}$$

Precipitation volume was calculated according to equation 6 using a runoff coefficient of 0.9.

$$\text{Precipitation Volume} = \text{Depth} * \text{Catchment Area} * \text{Runoff Coefficient} \qquad \text{Equation 6}$$

For each equalized flow event, a normalized effluent concentration was calculated according to equation 7.

$$\text{Normalized Effluent Conc.} = \frac{\text{Effluent Con.}}{\text{Influent Con.}} \qquad \text{Equation 7}$$

To determine any statistically significant differences between the sand and biochar effluent concentrations and ratios, a two-tailed student t-test using unequal variance was conducted. Significance was determined using a Pearson's p Analysis for p-value < 0.05.

3. Results and Discussion

3.1 Biochar Characterization

The contaminant removal performance of biochar is greatly influenced by its physical and chemical properties, which in turn are affected by feedstock type and pyrolysis temperature. Therefore, the composition of biochar is an important indicator of its physicochemical characteristics and contaminant removal performance for stormwater treatment needs. Table 5 provides the chemical characteristics of the red pine biochar produced at 550°C as compared to a commercial biochar (ABC char) obtained from American Biochar Company (investigated by Valenca et al. 2021).

Table 5. Biochar Characterization Results

Parameter	Red pine	ABC Char
Moisture total (wt%)	3.03	8.75
Ash (wt%)	1.52	12.00
Volatile matter (wt%)	80.15	79.51
Fixed carbon by difference (wt%)	18.33	8.5
Sulfur (wt%)	0.012	0.029
SO_2 (lb/mmbtu)	0.016	0.049
Gross Cal. Value at Const. vol. (btu/lb)	14372	11922
Carbon (C) (wt%)	77.86	80.59
Hydrogen (H) (wt%)	3.12	0.65
Nitrogen (N) (wt%)	0.84	0.75

Oxygen (O) (wt%)	16.66	5.99
H/C	0.481	0.097
O/C	2.57	0.892
(O+N)/C	0.290	0.167
Cumulative Pore Vol. (mL/g, 0-100nm)	0.369	0.443
Micropores (mL/g, PD < 2 nm)	0.111	0.214
Mesopores (mL/g, 2- 50 nm	0.238	0.222
Macropores (mL/g, > 50 nm)	2.95	1.96
pH in DI water (biochar/water)	8.64	9.67

The hydrogen (H) and oxygen (O) content of red pine biochar produced at 550 °C was higher than that of ABC char produced between 550 and 900^{o}C. Interestingly, all atomic ratios [i.e., H/C, O/C and (O+N)/ C] were higher for the red pine biochar as compared to the ABC char. Thus, red pine biochar showed lower aromaticity (H/C ratio) and polarity [O/C and (O+N)/C ratios], which could be attributable to the relatively low pyrolysis temperature. Increases in pyrolysis temperature results in lower H and O content, presumably due to the decomposition of the oxygenated bonds and loss of H and O containing functional groups (Guo et al. 2017).

The cumulative PSD curves (Figures 9-12, Appendix) show that pore volume (< 100 um) of the red pine biochar was slightly lower than that of the ABC char (Table 5). Biochar's high total pore volume makes it suitable for amending filtration media, contributing to the effective removal of stormwater pollutants particularly *E. Coli* and organic contaminants. The volume distribution between micro-, macro-, and mesopores is given in Table 5. The volume distribution revealed that the red pine biochar is characterized by macropores, while the ABC char has nearly double the volume of micropores. Overall, pore volume analysis revealed that red pine biochar had relatively lower micropores and higher macropores than ABC char with comparable mesopores.

Both the red pine and commercial biochars were alkaline (pH > 7). The pH value and ash content of red pine biochar were lower than the values observed for the ABC char. The increase in pH may be attributed to the enrichment of basic functional groups, decomposition of the organic matrix, as well as increasing concentrations of inorganic

cations (such as potassium, sodium, calcium, and magnesium) in the ash fraction (Weber and Quiker, 2018).

3.2 Hydraulic Conditions and Flow Distribution

Figure 6 shows the precipitation depths and system influent discharge from the parking lot weir for the 2022 field season. The level logger was placed in the parking lot weir box on May 3, 2022, and recorded data through September 27, 2022. The cumulative precipitation volume during this period was 417 m^3 while the cumulative measured discharge from the influent weir was 231 m^3, 55% of the precipitation volume with the remaining 45% flooding and bypassing the influent weir.

A total of 97 rain events were recorded in 2022 ranging in depth from 0.01 cm (the minimum recordable depth) to 3.79 cm, with 0.01 cm being recorded for 11 events. The three largest precipitation events occurred on May 11th (3.79 cm), August 12th (2.67 cm), and August 28th, (2.52 cm), resulting in cumulative daily discharges of 29 – 38 m^3. During larger precipitation events, the precipitation volume exceeded the cumulative measured discharge due to flooding of the system. As the system was designed for research to allow the comparison between multiple test beds rather than sized to the catchment area, this type of behavior is expected during peak flow.

Water quality data was collected for 11 precipitation events between April and August 2022. Table 6 shows the precipitation depths and flow distribution between the filter testbeds for sampling events. For sampled events, precipitation depth ranged from 0.18 cm on June 13th to 2.67 cm on August 12th. The resultant measured daily influent discharge volume ranged from 0.06 m^3 on June 13th to 31.47 m^3 on August 12th. Note that the time of sampling did not necessarily coincide with peak flow, and discharge data is recorded for the 20-minute duration over which sampling was being conducted. Therefore, larger precipitation events do not necessarily correlate with increased outflow. Brick orientation within the flow path primarily directed flow to the testbeds containing sand and biochar. The June 13th sampling event is the exception having the lowest

precipitation depth and total outflow discharge (Figure 6, Table 6). During this event, inflow to the filters was not high enough to reach the sand or biochar filter testbeds.

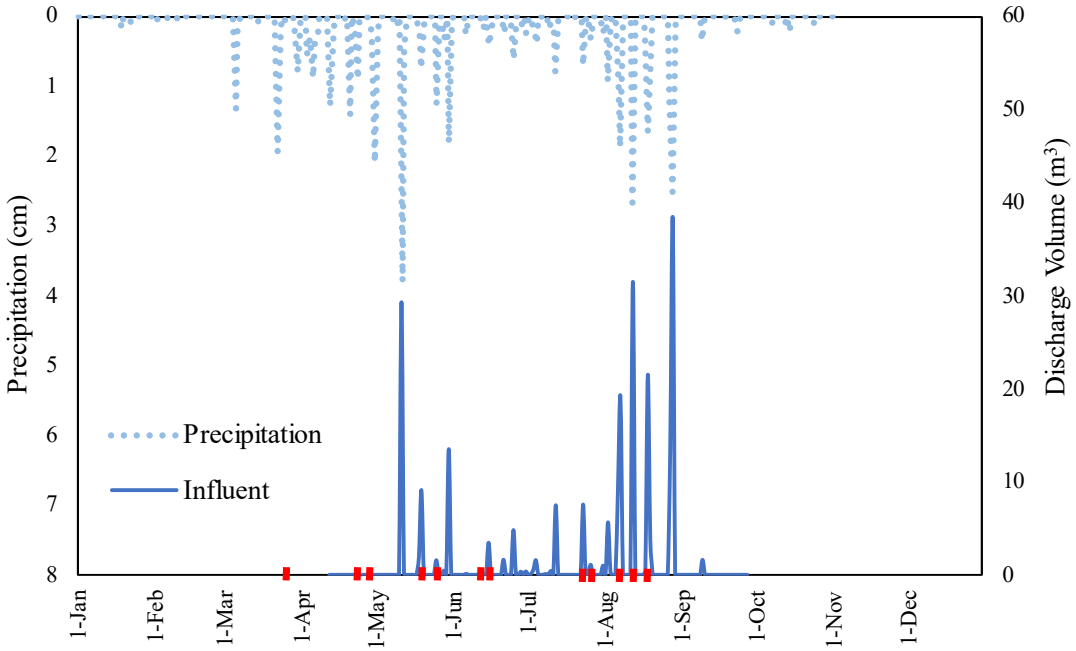

Figure 6. 2022 Precipitation and Measured Influent Volume
Precipitation depth is measured by the MWMO automated rain gauge and presented in cm. The influent discharge, measured in the weir box collecting parking lot run off, is presented as the cumulative daily volume in m^3. Red dashes along the x-axis indicate sampled events.

As little flow was directed to the IES filter during the 2022 sampling season, our analysis is focused on comparison of the sand and biochar testbeds. The flow distribution between the sand and biochar testbeds varied throughout the season such that flow equalization was not achieved for several events. To facilitate appropriate comparisons across systems undergoing similar flow conditions, further analysis is focused on events where flow was relatively equalized within 25% between the sand and biochar filters. For the duration of this paper, flow equalization is defined as equalization within 25%. The 6 flow equalized events are indicated with asterisks in Table 6.

Hydrographs and event characteristics of the 6 flow equalized sampling events are shown in Figure 7 and Table 6 respectively. Relative flow equalization occurred on the following sampling events: April 20th, April 30th, May 19th, June 15th, August 12th, and August 17th. Precipitation depth for flow equalized events ranged from 0.19 cm on

August 17th to 2.67 cm on August 12th. The system discharge volumes ranged from 0.45 m^3 to 31.47 m^3 for the influent, 0.22 m^3 to 6.12 m^3 for the sand, and 0.62 m^3 to 6.29 m^3 for the biochar on August 17th and August 12th respectively.

Table 6. 2022 Sample Date Flow Distribution Between Filters
Presented below are the precipitation, total outflow, and flow distribution for each sampling event in 2022 with measured discharge. The total outflow was calculated via the summation of each filter testbed at the time of sampling. Flow distributions were calculated at the time of sampling for each event according to equation 2. Asterisks indicate events during which a relative degree of flow equalization was achieved (±25%) and are the focus of further analysis.

Date	Precipitation (cm)	Total Outflow (L/min)	Sand	Biochar	IES
4/20/2022*	1.41	9.57	53%	46%	0%
4/30/2022*	2.09	10.46	47%	53%	0%
5/19/2022*	0.75	22.55	41%	54%	5%
5/25/2022	1.26	15.63	37%	63%	0%
6/13/2022	0.18	2.52	0%	0%	100%
6/15/2022*	0.42	30.74	46%	40%	14%
7/23/2022	0.69	19.13	0%	100%	0%
7/26/2022	0.33	31.41	19%	64%	17%
8/6/2022	0.96	33.32	--	86%	14%
8/12/2022*	2.67	7.31	54%	43%	2%
8/17/2022*	0.19	16.72	27%	52%	21%

Figure 7 shows the time of sampling during the precipitation event. Due to the inherent uncertainty in storm events and timing limitations, the time at which samples were taken did not always coincide with peak flows. Samples on April 20th, May 19th, and June 15th were taken near the beginning of their respective precipitation events while samples for April 30th, August 12th, and August 17th were taken following one or more peaks in flow. The sampling events in April are shown without influent discharge as the influent data logger was not installed until May 5th, 2022. As filter performance is analyzed according

to normalized concentrations for events that have achieved relative flow equalization, influent flow data is not required for analysis.

Sampling events on May 19th and August 12th show peak influent discharge over 1,000 L/min greater than effluent discharge. The August 12th event is the largest precipitation event in 2022 with a depth of 2.67 cm and volume of 31.5 m^3. The antecedent precipitation event, while 5 days beforehand, was also large at 1.86 cm and 27.8 m^3. Volume retained from the large antecedent event in the filter testbeds combined with the large sampling event led to significant flooding and low effluent discharge. While the May 25th sampling and antecedent events were less than half of those seen on August 12th, the antecedent precipitation occurred within less than 24 hours of the sampling event. As such, a greater percentage of the antecedent precipitation volume was retained within the filter testbeds resulting in similar flooding conditions and low effluent discharge.

On average, less than 40% of precipitation volumes are exiting the system through the filter testbeds. The June 15th event is an exception to this trend with 81% of precipitation volume becoming filter effluent. This event had the second lowest precipitation of the sampled events resulting in greater volumes of precipitation not reaching the sand and biochar filters and instead entering the IES filter. This, combined with a low antecedent precipitation having occurred over 24 hours beforehand, resulted in significantly less flooding compared to other sampled events.

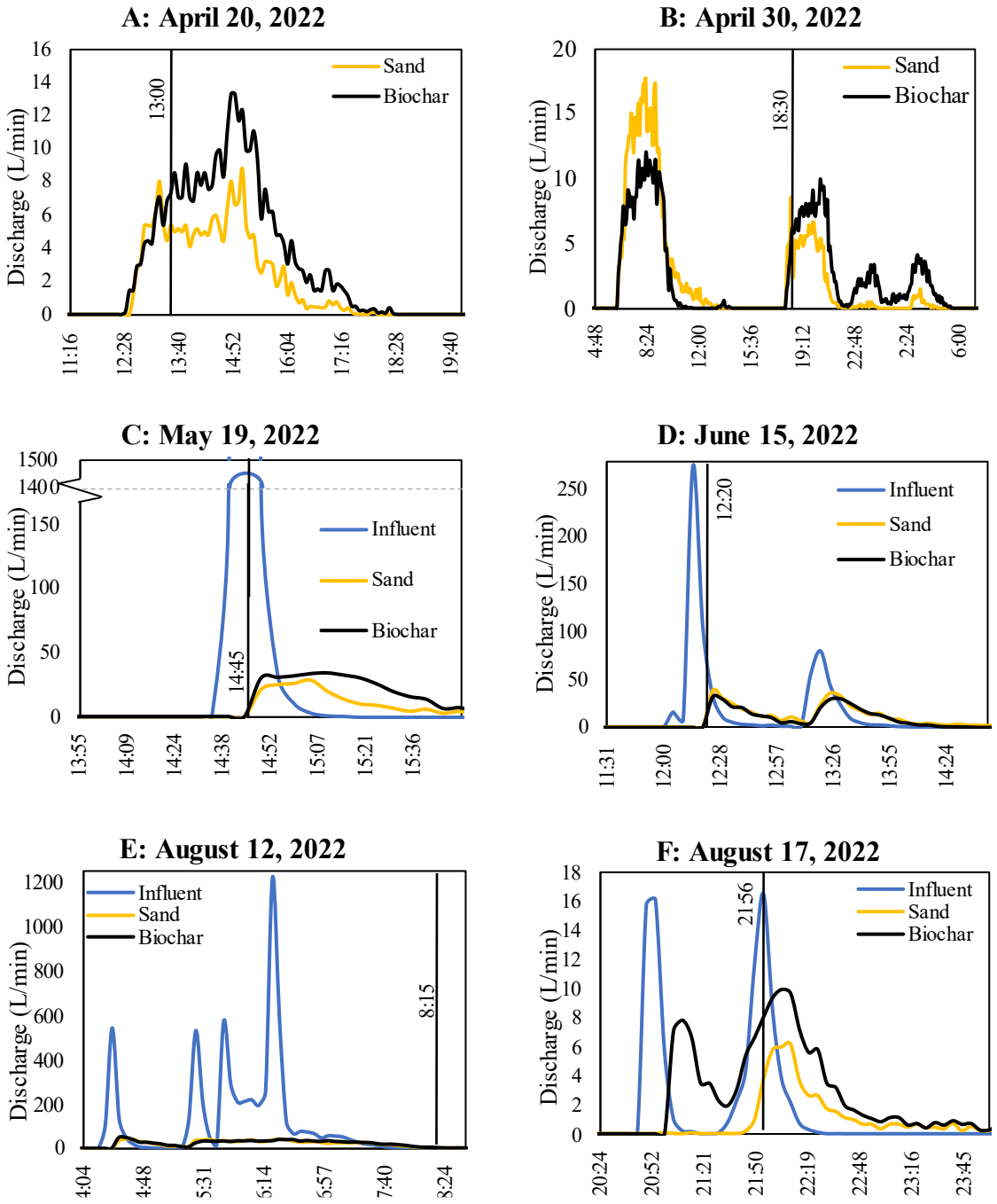

Figure 7. Hydrographs of 2022 Flow Equalized Events

A through F show the hydrographs for the 6 flow equalized events that occurred in 2022- April 20, April 30, May 19, June 15, August 12, and August 17 respectively. The hydrographs show discharge in L/min with a line indicating the time of sampling.

Table 7. Characteristics of 2022 Flow Equalized Events
Presented here are characteristics of the 2022 flow equalized events shown in Figure 7. Precipitation volumes are calculated according to equation 6. Event measured influent is a summation of volume over the entire event. Total Event Outflow/Precipitation is the percentage of event precipitation being treated and exiting the system through the filter testbeds.

Date	20-Apr	30-Apr	19-May	15-Jun	12-Aug	17-Aug
Time Since Peak Inflow	--	--	0	15min	1hr 55min	1 min
Antecedent Dry Period	1 day	1hr 40min	18hr 50min	1 day	4 days	5 days
Antecedent Precipitation Depth (cm)	0.01	0.25	0.21	0.18	1.86	2.67
Antecedent Precipitation Volume (m^3)	0.15	3.79	3.14	2.73	27.81	39.89
Precipitation Depth (cm)	1.41	2.09	0.75	0.42	2.67	0.19
Precipitation Volume (m^3)	21.06	31.18	11.21	6.33	39.89	2.88
Event Measured Inflow (m^3)	--	--	9.11	3.44	31.47	0.45
Total Event Outflow/Precipitation Volume	13%	29%	27%	81%	36%	39%

3.3 Contaminant Removal Performance

To provide greater analysis of filter performance for flow equalized events, analysis of the normalized effluent concentration (C_{out}/C_{in}), which is the effluent concentration divided by the influent concentration at the time of sampling, is completed below. Table 8 shows the contaminant concentrations for the 6 flow equalized events. Figure 8 shows the normalized effluent concentration data as box and whisker plots.

Normalized effluent concentration values less than 1 indicate contaminant removal by filters. Both the sand and biochar filters provide removal of *E. coli*, TP, all metals, TOC, and TSS. The biochar filter removed minimal orthophosphate while the sand filter exported the contaminant. Both the sand and biochar exported nitrate, though the biochar to a lesser degree. A Pearson's p analysis was conducted between the sand and biochar

filter performances for all contaminants. P-values ranged from 0.4627 for nitrate and 0.9960 for copper, finding no statistically significant difference between the sand and biochar filter performances for 2022 flow equalized events (Table 16 in the Appendix).

Table 8. Contaminant Concentrations for 2022 Flow Equalized Events
Shown below are contaminant concentrations sampled during flow equalized events for each constituent. Values marked with an asterisk indicate normalized effluent concentration outliers. Italicized values indicate concentrations below the detection limit.

		20-Apr	30-Apr	19-May	15-Jun	12-Aug	17-Aug
E. coli (MPN/100L)	Influent	3		1553	38300	539	63
	Sand	5*		291	13500	46	1
	Biochar	5*		147	14800	20	44
TP (mg/L)	Influent	0.142	0.0905	0.1845	1.112	0.0505	0.2815
	Sand	0.045	0.038	0.0685	0.259	0.1355*	0.1235
	Biochar	0.025	0.039	0.0595	0.2935	0.148*	0.183
Ortho P (mg/L)	Influent	0.037	*0.01*		0.607		0.039
	Sand	0.014	0.03		0.02		0.11
	Biochar	*0.01*	0.015		0.056		0.128
Nitrate (mg/L N)	Influent	2.19	0.48	0.59	*0.2*	*0.2*	0.52
	Sand	1.26	0.32	2.15	2.92*	0.25	0.65
	Biochar	0.72	0.41	*0.2*	0.28	0.74	2.25
Nickel (ug/L)	Influent	3.7	1.7	2.3	9.6	*0.5*	2.2
	Sand	1.3	0.99	3.2	6.4	*0.5*	0.51
	Biochar	1.1	0.59	4.1		*0.5*	0.83
Copper (ug/L)	Influent	12.5	7.9	11.8	41	2.5	10.5
	Sand	7.4	4.8	7.8	15.4	2.5*	2.6
	Biochar	6.2	3.3	4.6		3.2*	3.3
Zinc (ug/L)	Influent	101	66.3	129	406	25	65.3
	Sand	16.2	19.2	95.3	139	5.8	42.3
	Biochar	35	7	73.5*		*5*	22
TOC (mg/L)	Influent	41.9	11.7	10.4	74.4		27.2
	Sand	14	2.7	14.3*	34.6		2.9
	Biochar	13.3	2.4	12.6*	38.4		12.2
TSS (mg/L)	Influent	31	28	80	179	6	19
	Sand	4	9	5	15	*3*	*3*
	Biochar	4	*3*	4	13	*3**	*3*

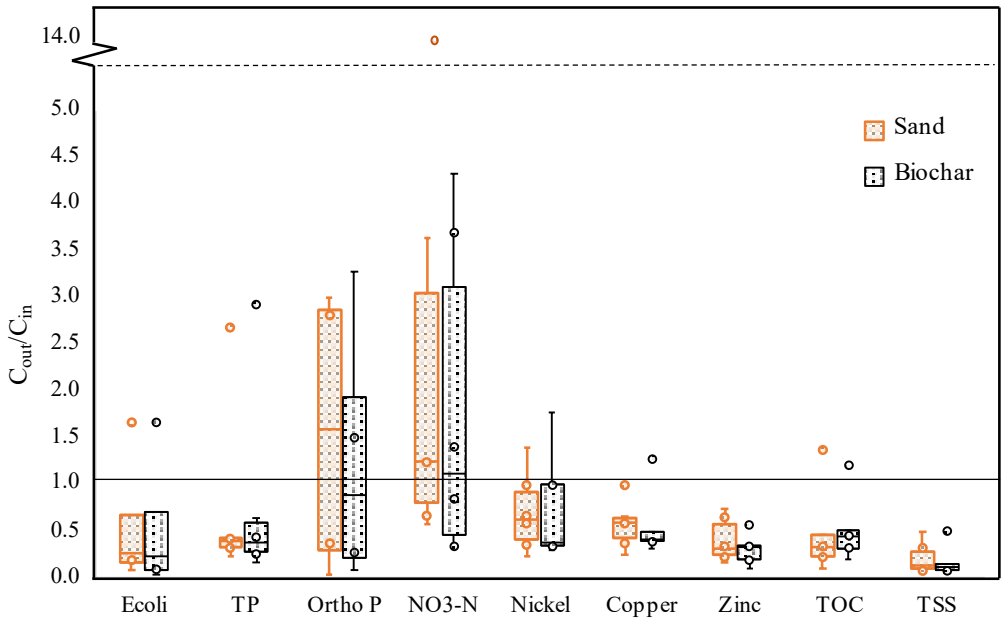

Figure 8 Normalized Effluent Concentrations for 2022 Equalized Flow Events
Box and whisker plots show the normalized effluent concentrations for flow equalized events. Values greater than 1 indicate contaminant export, and values less than 1 indicate removal. Plots use the inclusive median and display inner points and event outliers. Outliers are calculated using the interquartile range method. Outlier events are noted with an asterisk in Table 8.

3.3.1 E. coli Removal Performance

Both the sand and biochar filters provide removal of *E. coli* with normalized effluent concentrations ranging from 0.02 to 1.67 for the sand filter and from 0.04 to 1.67 for the biochar filter. The maximum normalized effluent concentration values for both the sand and biochar filters, 1.67, occurred on April 20th. These values were determined to be outliers and are the only values indicating export of *E. coli* for flow equalized events. The influent concentration for this event was 3 MPN/100mL while most other events exceeded 500 MPN/100mL. Additionally, export of this event was minimal with effluent concentrations only rising to 5 MPN/100mL. It is possible that minimal mobilization within the filters exceeded the substantially low influent concentrations causing a large normalized effluent concentration. No significant difference was found between the sand and biochar filter performances (p-value = 0.7942) indicating the filters obtained similar *E. coli* removal performance through the 2022 field season.

Improvements to filter performance upon the addition of biochar have been seen in literature. Studies by Mohanty and Boehm (2014) and Lau et al. (2017) found a statistically significant improvement in *E. coli* removal for biochar columns compared to sand only columns with removal above 90%. Both studies used biochars produced at temperatures higher than the biochar used in the MWMO filter testbeds. One study compared the performance of biochars produced at low and high temperatures from two feedstock types (Abit et al. 2014). Here, the high temperature biochar of both feedstocks and the low temperature biochar from one feedstock provided significant improvement compared to sand columns for *E. coli* removal. The second low temperature biochar, produced for the second feedstock type, decreased *E. coli* removal and exported the contaminant. Results from this study emphasize the importance of not only pyrolysis temperature but also feedstock type in the development of biochar characteristics for water quality improvements.

A recent study compared the performance of four commercial biochars for *E. coli* removal and examined which biochar properties were correlated with greatest contaminant removal (Valenca et al. 2021). Researchers found a positive correlation between the *E. coli* removal capacity of biochar and surface area and fixed carbon content. Biochar properties such as ash content and volatile organic matter were found to be negatively correlated with *E. coli* removal capacity. Surface area and fixed carbon have been shown to increase with increasing pyrolysis temperature (Uchimiya et al. 2011; Valenca et al. 2021). As fixed carbon content contributes to a biochar's hydrophobicity, higher temperature biochars are able to maintain the hydrophobic and steric interactions known to remove *E. coli* (Abit et al. 2014; Mohanty and Boehm 2014; Afrooz and Boehm 2016). The volatile matter content of a biochar has also been shown to decrease with increasing pyrolysis temperature (Uchimiya et al. 2011). The properties shown to improve *E. coli* removal capacity are more prevalent in higher temperature biochars. As such, had a higher temperature biochar been used in the MWMO filter test beds, improvements in *E. coli* removal may have been seen.

3.3.2 Phosphorus Removal Performance

Both the sand and biochar filters provided removal of TP. Normalized effluent concentrations ranged from 0.23 to 2.68 for the sand filter and from 0.18 to 2.93 for the biochar filter. The maximum normalized effluent concentrations for both the sand and biochar occurred on August 12th and were determined to be outliers. August 12th is the only event indicating export of TP for flow equalized events. The influent TP concentration on August 12th was the lowest of the 6 analyzed events. The August 12th precipitation event occurred later in the field season and was the largest sampled event. It is likely that export occurred due to accumulation of phosphorus within the filters throughout the year and subsequent flushing out of the system by the large precipitation event. No significant difference between the sand and biochar filter performance was found (p-value = 0.9307). These results indicate the filters obtained similar TP removal performance through the 2022 field season.

The sand and biochar filter did not provide consistent removal of orthophosphate, with normalized effluent concentrations ranging from 0.03 to 3.0 and 0.09 to 3.28 respectively. No outliers in performance were found for either filter. No significant difference between the sand and biochar filter performance was found (p-value = 0.8089). These results indicate the filters obtained similar orthophosphate removal performance through the 2022 field season.

Phosphorus species possess negative charges leading to repulsion in sand media (Grebel et al. 2013; Chen et al. 2022). Medias containing iron oxides, like iron enhanced sand (IES), provide significantly greater removal of phosphorus in comparison to sand and biochar medias (Erickson et al. 2007; Grebel et al. 2013; Fischer and Feinberg 2019; Erickson et al. 2021). The positively charged iron oxides in IES remove phosphate species through electrostatic adsorption (Fischer and Feinberg 2019). Improvements in phosphorus removal upon biochar amendment is inconsistent in literature (Mohanty et al. 2018; Chen et al. 2022). As negatively charged sand medias repel negatively charged contaminants, the likely mechanism of removal in the sand and biochar filters is physical straining. However, dissolved species are not likely to strain in filter media (Erickson et

al. 2007). Because TP is composed of both particulate and dissolved phosphorus species, straining of particulate phosphorus is responsible for TP removal.

Additionally, large quantities of particulate phosphorus are known to bind to sediments in stormwater (Sansalone and Kim 2008; Berretta and Sansalone 2011). Both filters provide considerable removal of TSS, likely leading to greater reduction of bound particulate phosphorus. Potential improvements in TP and TSS removal by the biochar-amended filters are likely due to increased porosity and straining capacity in biochar caused by finer particles not seen in sand that can fill spaces between larger media particles. (Mohanty and Boehm 2014). Greater porosity and surface area provide greater opportunities for adsorption of dissolved species (Arias et al. 2001; Bock et al. 2015). It is also be possible for Mg and Ca inherent to biochar to form insoluble phosphorus precipitates (Yao et al. 2011; Bock et al. 2015).

3.3.3 Nitrate Removal Performance

Neither the sand nor the biochar filter provided consistent removal of nitrate, with both filters exporting the contaminant for the majority of sampling events. Normalized effluent concentrations ranged from 0.58 to 14.6 for the sand filter. The biochar filter provided lowered export, with normalized effluent concentrations ranging from 0.33 to 4.33. The maximum normalized effluent concentration for the sand filter occurred on June 15th and was identified as an outlier. No outliers were found for the biochar filter. The exceptionally large export by the sand filter on June 15th is likely due to the low influent concentration, below the detention limit. Nitrate retained within the filter from the antecedent precipitation on June 13th was likely flushed out of the system on June 15th and exceeded the low influent concentration. It is also possible for nitrification to have occurred in the system, as Table 46 in the Appendix shows decreased effluent ammonia concentrations for several events. No significant difference was found between the sand and biochar filter performance (p-value = 0.4627). These results indicate the filters obtained similar export of nitrate through the 2022 field season.

The removal of nitrate by biochar is inconsistent in literature (Xu et al. 2016; Ulrich et al. 2017; Mohanty et al. 2018; Tian et al. 2019; Chen et al. 2022). One biochar produced via gasification showed significant improvement in nitrate removal (Ulrich et al. 2017). Two other studies using biochar produced near 550^{o}C showed reduced nitrate leaching, as seen in the MWMO filter test beds, and significant removal in combination with iron materials (Xu et al. 2016; Tian et al. 2019). Improved filter performance for nitrate removal upon the addition of biochar can be partially attributed to improved water retention capacity. Increased water retention capacity allows for micro-anoxic environments to form, promoting denitrification (Ulrich et al. 2017; Tian et al. 2019). Biochar also provides greater porosity and high specific surface area, leading to potential reaeration of the filter media for greater microbial activity (Xu et al. 2016). More importantly, biochar is able to act as an electron carrier for bacteria during the denitrification process either through conductive means or the redox of quinone groups with intermediate and high temperature biochars possessing the greatest ability to accept and donate electrons. (Klüpfel et al. 2014; Saquing et al. 2016; Ulrich et al. 2017). Biochars produced at intermediate and high temperatures possess the greatest ability to accept and donate electrons (Klüpfel et al. 2014). As several of the biochar characteristics responsible for improved nitrate removal occur at higher temperatures, a higher temperature biochar may be able to provide greater filter performance against nitrate than that seen in the MWMO filter testbeds.

3.3.4 Metal Removal Performance

Both the sand and biochar filters provided consistent removal of zinc, copper, and nickel. Of the metals analyzed here, filters showed the greatest removal of zinc, with normalized effluent concentrations ranging from 0.16 to 0.74 for the sand filter and 0.11 to 0.57 for the biochar filter. For copper, normalized effluent concentrations ranged from 0.25 to 1.0 for the sand filter and 0.31 to 1.28 for the biochar filter. While still providing consistent removal, filters showed a lowered affinity for nickel with normalized effluent concentrations ranging from 0.23 to 1.39 for the sand filter and 0.30 to 1.78 for the biochar filter.

An outlier for biochar performance against zinc was found on May 19th where influent concentrations were nearly double that of other sampled events, likely overwhelming the system. The August 12th event was identified as a copper performance outlier for both the sand and biochar. The August 12th event contained the lowest influent concentration at 2.5 ug/L of copper. The sand and biochar filter provide no to minimal export with effluent concentrations of 2.5 ug/L and 3.2 ug/L respectively. As August 12th was the largest sampled precipitation event, it is likely that the system was overwhelmed, and minimal export exceeded low influent concentrations. No significant difference was found between the sand and biochar filter performances for the metals analyzed with p-values of 0.4868, 0.9960, and 0.8702 for zinc, copper, and nickel respectively. Therefore, these results show that both the sand and biochar filters obtained similar metal removal performance through the 2022 field season.

Removal of metals by conventional filtration media and biochar is well documented in literature (Hatt et al. 2008; Liu and Zhang 2009; Gwenzi et al. 2017; Mohanty et al. 2018; Boehm et al. 2020; Chen et al. 2022). Here, minimal to no improvement is seen with the addition of biochar. Removal mechanisms of metals in filtration media are species dependent, though the most common mechanisms in negatively charged sand medias are sorption and electrostatic interaction with negatively charged surface functional groups (Reddy et al. 2014; Li et al. 2017). Low and intermediate temperature biochars, like the one used in the MWMO filter testbeds, favor metal removal due to higher cation exchange capacities and greater quantities of oxygen containing functional groups. Additionally, large quantities of metals are known to be bound to particulate matter in stormwater (Hatt et al. 2007). These metals are removed with sediments.

Lab studies using biochar have seen removal capacities as high as 80% to greater than 95% removal for heavy metals (Kołodyńska et al. 2012; Alslaibi et al. 2014; Mahdi et al. 2018). Contrary to the MWMO filter testbeds, the media in these studies received influent only containing heavy metals. Two studies using sand filtration media found similarly large removal for Cu and Zn (Hatt et al. 2007; Hatt et al. 2008). In these studies, media was dosed with synthetic stormwater containing sediments and nutrients in combination with heavy metals. However, unlike the MWMO filter test beds, the

filtration media was artificially aged with clean water. One lab study using influent containing synthetic stormwater with metals, nutrients, and organics without media aging showed similar or lower removal to that seen by the MWMO filter testbeds (Reddy et al. 2014). It is likely that the complex mixture of contaminants in natural stormwater creates greater competition for adsorption sites. This competition in addition to aging leads to lowered removal of heavy metals. These results show the difficulty and necessity of mimicking field conditions in the lab.

3.3.5 TOC Removal Performance

Both the sand and biochar filters provided consistent removal of TOC with normalized effluent concentrations ranging from 0.11 to 1.38 for the sand filter and 0.21 to 1.21 for the biochar filter. The maximum normalized effluent concentrations for both filters were identified as outliers, having been the only event indicating export of TOC. The outliers both occurred on the May 19th sampling event. No significant difference was found between the sand and biochar filter performances with a p-value of 0.8995, indicating the sand and biochar obtained similar TOC removal performance through the 2022 field season.

The removal of organics by both sand-only and biochar-amended sand is variable in literature dependent on biochar and contaminant characteristics (Ulrich et al. 2015; Ulrich et al. 2017; Mohanty et al. 2018; Boehm et al. 2020; Chen et al. 2022). Sorption of organic carbons is controlled by hydrophobic interactions with greater removal of hydrophobic and nonpolar organics than polar organics (Ulrich et al. 2017; Saiz-Rubio et al. 2019; Boehm et al. 2020). Higher temperature biochars contain larger numbers of hydrophobic functional groups and as such may have shown a greater improvement in TOC removal had it been used in the MWMO filter test beds.

3.3.6 TSS Removal Performance

The sand and biochar filters provided the greatest and most consistent removal of TSS with normalized effluent concentrations ranging from 0.06 to 0.50 for the sand filter and

from 0.05 to 0.50 for the biochar filter. The maximum normalized effluent concentration for the biochar, 0.50 on August 12th, was identified as an outlier. The influent concentration was very low for this event at 6 mg/L. The biochar filter reduced the TSS concentration to below the detection limit of 3 mg/L. However, because this is only half of the influent concentration, the resultant normalized effluent concentration is large. As both filters provided exceptional removal of TSS, no significant difference was found between the sand and biochar filter performances (p-value = 0.6911). These results indicate the sand and biochar filters obtained similar TSS removal performance through the 2022 field season.

Traditional filtration provides excellent removal of sediments, and as such, the addition of biochar provides minimal improvement to the system (Hatt et al. 2007; Hatt et al. 2008; Payne et al. 2014; Boehm et al. 2020). Suspended solids are typically removed via straining and settling, with media containing similar particle distribution as stormwater solids providing the greatest removal (Hatt et al. 2007; Hatt et al. 2008). As large quantities of particulate contaminants can be bound to suspended sediments, the removal TSS assists the removal of other contaminants as seen in the MWMO filter test beds for particulate phosphorus and metals (Hatt et al. 2007; Sansalone and Kim 2008).

4. Conclusions

In this study, the performance of catchment-scale sand and biochar amended filters were analyzed. Filters were sampled 26 times over 2 years, with the 2022 field season being the focus of the analysis presented herein. Six events from the 2022 field season showed flow equalization between the sand and biochar filters within 25% and were used for detailed performance analysis. Both filters provided removal of *E. coli,* TP, metals, TOC, and TSS. The sand and biochar provided inconsistent removal of orthophosphate. Both filters exported nitrate, though the biochar filter to a lesser degree. The addition of biochar provided greater decreases in concentration for zinc and TSS though no statistically significant difference between the sand and biochar was found for any filter performance. Most notable was the removal of *E. coli* and phosphorus species and the

prevention of excessive nitrate export by the biochar filter. These results demonstrate the potential for removal of *E. coli* and dissolved nutrient species. Greater improvements may be seen using a biochar produced at higher temperatures due to increased hydrophobicity, porosity, and water retention. Because of the variability of biochar amended filter performance seen in this study and literature, it is recommended that performance of biochar-amended media be tested prior to deployment in the field to ensure ideal media characteristics have been selected for the target contaminants. Additionally, differences between field performance and literature show the importance of mimicking field conditions in the lab and conducting biochar research in the field. The complex mixture of contaminants within urban stormwater and the effects of field aging must be analyzed to determine the true removal capacities of biochar-amended media.

5. References

Abit SM, Bolster CH, Cantrell KB, Flores JQ, Walker SL. 2014. Transport of *Escherichia coli*, *Salmonella typhimurium* , and Microspheres in Biochar-Amended Soils with Different Textures. J Environ Qual. 43(1):371–388. doi:10.2134/jeq2013.06.0236.

Afrooz ARMN, Boehm AB. 2016. Escherichia coli Removal in Biochar-Modified Biofilters: Effects of Biofilm. Nerenberg R, editor. PLOS ONE. 11(12):e0167489. doi:10.1371/journal.pone.0167489.

Alslaibi T, Abustan I, Ahmad M, Foul A. 2014. Preparation of Activated Carbon From Olive Stone Waste: Optimization Study on the Removal of Cu2+, Cd2+, Ni2+, Pb2+, Fe2+, and Zn2+ from Aqueous Solution Using Response Surface Methodology. J Dispers Sci Technol. 35(7):913–925. doi:10.1080/01932691.2013.809506.

Arias CA, Del Bubba M, Brix H. 2001. Phosphorus removal by sands for use as media in subsurface flow constructed reed beds. Water Res. 35(5):1159–1168. doi:10.1016/S0043-1354(00)00368-7.

Barnes RT, Gallagher ME, Masiello CA, Liu Z, Dugan B. 2014. Biochar-Induced Changes in Soil Hydraulic Conductivity and Dissolved Nutrient Fluxes Constrained by Laboratory Experiments. Zhou Z, editor. PLoS ONE. 9(9):e108340. doi:10.1371/journal.pone.0108340.

Berretta C, Sansalone J. 2011. Hydrologic transport and partitioning of phosphorus fractions. J Hydrol. 403(1–2):25–36. doi:10.1016/j.jhydrol.2011.03.035.

Bock E, Smith N, Rogers M, Coleman B, Reiter M, Benham B, Easton ZM. 2015. Enhanced Nitrate and Phosphate Removal in a Denitrifying Bioreactor with Biochar. J Environ Qual. 44(2):605–613. doi:10.2134/jeq2014.03.0111.

Boehm AB, Bell CD, Fitzgerald NJM, Gallo E, Higgins CP, Hogue TS, Luthy RG, Portmann AC, Ulrich BA, Wolfand JM. 2020. Biochar-augmented biofilters to improve pollutant removal from stormwater – can they improve receiving water quality? Environ Sci Water Res Technol. 6(6):1520–1537. doi:10.1039/D0EW00027B.

Chen Y, Wu Q, Tang Y, Liu Z, Ye L, Chen R, Yuan S. 2022. Application of biochar as an innovative soil ameliorant in bioretention system for stormwater treatment: A review of performance and its influencing factors. Water Sci Technol. 86(5):1232–1252. doi:10.2166/wst.2022.245.

Deng Y. 2020. Low-cost adsorbents for urban stormwater pollution control. Front Environ Sci Eng. 14(5):83. doi:10.1007/s11783-020-1262-9.

Ekanayake D, Loganathan P, Johir MAH, Kandasamy J, Vigneswaran S. 2021. Enhanced Removal of Nutrients, Heavy Metals, and PAH from Synthetic Stormwater by Incorporating Different Adsorbents into a Filter Media. Water Air Soil Pollut. 232(3):96. doi:10.1007/s11270-021-05059-6.

EPA. 2009. Industrial Stormwater Monitoring and Sampling Guide.

Erickson A, Kozarek J, Kramarczuk K, Lewis L. 2021. Biofiltration Media Optimization - Phase 1 Final Report. Final Rep.:70.

Erickson AJ, Gulliver JS, Weiss PT. 2007. Enhanced Sand Filtration for Storm Water Phosphorus Removal. J Environ Eng. 133(5):485–497. doi:10.1061/(ASCE)0733-9372(2007)133:5(485).

Fischer B, Feinberg J. 2019. Formation pathways for iron oxide minearls and geochemical conditions for phosphate retention in iron enhanced sand filters. [accessed 2022 Oct 4]. https://www.wrc.umn.edu/sites/wrc.umn.edu/files/2019-11_fisher_feinberg_swrc_final_report_iesf_1.pdf.

Grebel JE, Mohanty SK, Torkelson AA, Boehm AB, Higgins CP, Maxwell RM, Nelson KL, Sedlak DL. 2013. Engineered Infiltration Systems for Urban Stormwater Reclamation. Environ Eng Sci. 30(8):437–454. doi:10.1089/ees.2012.0312.

Gwenzi W, Chaukura N, Noubactep C, Mukome FND. 2017. Biochar-based water treatment systems as a potential low-cost and sustainable technology for clean water provision. J Environ Manage. 197:732–749. doi:10.1016/j.jenvman.2017.03.087.

Hale SE, Lehmann J, Rutherford D, Zimmerman AR, Bachmann RT, Shitumbanuma V, O'Toole A, Sundqvist KL, Arp HPH, Cornelissen G. 2012. Quantifying the Total and Bioavailable Polycyclic Aromatic Hydrocarbons and Dioxins in Biochars. Environ Sci Technol. 46(5):2830–2838. doi:10.1021/es203984k.

Hatt BE, Deletic A, Fletcher TD. 2007. Stormwater reuse: designing biofiltration systems for reliable treatment. Water Sci Technol. 55(4):201–209. doi:10.2166/wst.2007.110.

Hatt BE, Fletcher TD, Deletic A. 2008. Hydraulic and Pollutant Removal Performance of Fine Media Stormwater Filtration Systems. Environ Sci Technol. 42(7):2535–2541. doi:10.1021/es071264p.

Hettiarachchi S, Wasko C, Sharma A. 2018. Increase in flood risk resulting from climate change in a developed urban watershed – the role of storm temporal patterns. Hydrol Earth Syst Sci. 22(3):2041–2056. doi:10.5194/hess-22-2041-2018.

Klüpfel L, Keiluweit M, Kleber M, Sander M. 2014. Redox Properties of Plant Biomass-Derived Black Carbon (Biochar). Environ Sci Technol. 48(10):5601–5611. doi:10.1021/es500906d.

Kołodyńska D, Wnętrzak R, Leahy JJ, Hayes MHB, Kwapiński W, Hubicki Z. 2012. Kinetic and adsorptive characterization of biochar in metal ions removal. Chem Eng J. 197:295–305. doi:10.1016/j.cej.2012.05.025.

Li H, Dong X, da Silva EB, de Oliveira LM, Chen Y, Ma LQ. 2017. Mechanisms of metal sorption by biochars: Biochar characteristics and modifications. Chemosphere. 178:466–478. doi:10.1016/j.chemosphere.2017.03.072.

Liu W-J, Jiang H, Yu H-Q. 2015. Development of Biochar-Based Functional Materials: Toward a Sustainable Platform Carbon Material. Chem Rev. 115(22):12251–12285. doi:10.1021/acs.chemrev.5b00195.

Liu Z, Zhang F-S. 2009. Removal of lead from water using biochars prepared from hydrothermal liquefaction of biomass. J Hazard Mater. 167(1–3):933–939. doi:10.1016/j.jhazmat.2009.01.085.

Mahdi Z, Yu QJ, El Hanandeh A. 2018. Investigation of the kinetics and mechanisms of nickel and copper ions adsorption from aqueous solutions by date seed derived biochar. J Environ Chem Eng. 6(1):1171–1181. doi:10.1016/j.jece.2018.01.021.

MN SSC. 2008. Minnesota Stormwater Manual. https://stormwater.pca.state.mn.us/images/b/b8/Minnesota_Stormwater_Manual.pdf.

Mohan D, Sarswat A, Ok YS, Pittman CU. 2014. Organic and inorganic contaminants removal from water with biochar, a renewable, low cost and sustainable adsorbent – A critical review. Bioresour Technol. 160:191–202. doi:10.1016/j.biortech.2014.01.120.

Mohanty SK, Boehm AB. 2014. *Escherichia coli* Removal in Biochar-Augmented Biofilter: Effect of Infiltration Rate, Initial Bacterial Concentration, Biochar Particle Size, and Presence of Compost. Environ Sci Technol. 48(19):11535–11542. doi:10.1021/es5033162.

Mohanty SK, Cantrell KB, Nelson KL, Boehm AB. 2014. Efficacy of biochar to remove Escherichia coli from stormwater under steady and intermittent flow. Water Res. 61:288–296. doi:10.1016/j.watres.2014.05.026.

Mohanty SK, Valenca R, Berger AW, Yu IKM, Xiong X, Saunders TM, Tsang DCW. 2018. Plenty of room for carbon on the ground: Potential applications of biochar for stormwater treatment. Sci Total Environ. 625:1644–1658. doi:10.1016/j.scitotenv.2018.01.037.

NRC, NAP, editors. 2009. Urban stormwater management in the United States. https://www3.epa.gov/npdes/pubs/nrc_stormwaterreport.pdf.

Panwar NL, Pawar A, Salvi BL. 2019. Comprehensive review on production and utilization of biochar. SN Appl Sci. 1(2):168. doi:10.1007/s42452-019-0172-6.

Payne EGI, Fletcher TD, Cook PLM, Deletic A, Hatt BE. 2014. Processes and Drivers of Nitrogen Removal in Stormwater Biofiltration. Crit Rev Environ Sci Technol. 44(7):796–846. doi:10.1080/10643389.2012.741310.

Qian K, Kumar A, Zhang H, Bellmer D, Huhnke R. 2015. Recent advances in utilization of biochar. Renew Sustain Energy Rev. 42:1055–1064. doi:10.1016/j.rser.2014.10.074.

Reddy KR, Xie T, Dastgheibi S. 2014. Evaluation of Biochar as a Potential Filter Media for the Removal of Mixed Contaminants from Urban Storm Water Runoff. J Environ Eng. 140(12):04014043. doi:10.1061/(ASCE)EE.1943-7870.0000872.

Saiz-Rubio R, Balseiro-Romero M, Antelo J, Díez E, Fiol S, Macías F. 2019. Biochar as low-cost sorbent of volatile fuel organic compounds: potential application to water remediation. Environ Sci Pollut Res. 26(12):11605–11617. doi:10.1007/s11356-018-3798-9.

Sansalone JJ, Kim J-Y. 2008. Transport of Particulate Matter Fractions in Urban Source Area Pavement Surface Runoff. J Environ Qual. 37(5):1883–1893. doi:10.2134/jeq2007.0495.

Saquing JM, Yu Y-H, Chiu PC. 2016. Wood-Derived Black Carbon (Biochar) as a Microbial Electron Donor and Acceptor. Environ Sci Technol Lett. 3(2):62–66. doi:10.1021/acs.estlett.5b00354.

Streuble J. 2015. Biochar: Physical and Chemical Characteristics. https://lpelc.org/agronomic-and-environmental-uses-of-biochar-part-1/.

Tian J, Jin J, Chiu PC, Cha DK, Guo M, Imhoff PT. 2019. A pilot-scale, bi-layer bioretention system with biochar and zero-valent iron for enhanced nitrate removal from stormwater. Water Res. 148:378–387. doi:10.1016/j.watres.2018.10.030.

Tirpak RA, Afrooz AN, Winston RJ, Valenca R, Schiff K, Mohanty SK. 2021. Conventional and amended bioretention soil media for targeted pollutant treatment: A critical review to guide the state of the practice. Water Res. 189:116648. doi:10.1016/j.watres.2020.116648.

Uchimiya M, Wartelle LH, Klasson KT, Fortier CA, Lima IM. 2011. Influence of Pyrolysis Temperature on Biochar Property and Function as a Heavy Metal Sorbent in Soil. J Agric Food Chem. 59(6):2501–2510. doi:10.1021/jf104206c.

Ulrich BA, Im EA, Werner D, Higgins CP. 2015. Biochar and Activated Carbon for Enhanced Trace Organic Contaminant Retention in Stormwater Infiltration Systems. Environ Sci Technol. 49(10):6222–6230. doi:10.1021/acs.est.5b00376.

Ulrich BA, Loehnert M, Higgins CP. 2017. Improved contaminant removal in vegetated stormwater biofilters amended with biochar. Environ Sci Water Res Technol. 3(4):726–734. doi:10.1039/C7EW00070G.

US EPA O. 2016. Climate Change Indicators: U.S. and Global Precipitation. [accessed 2022 Oct 12]. https://www.epa.gov/climate-indicators/climate-change-indicators-us-and-global-precipitation.

USBR. 2001. Chapter 7 - Weirs. In: Water Measurement Manual. 3rd ed. [accessed 2022 Oct 6]. https://www.usbr.gov/tsc/techreferences/mands/wmm/.

Valenca R, Borthakur A, Zu Y, Matthiesen EA, Stenstrom MK, Mohanty SK. 2021. Biochar Selection for *Escherichia coli* Removal in Stormwater Biofilters. J Environ Eng. 147(2):06020005. doi:10.1061/(ASCE)EE.1943-7870.0001843.

Veiga PA da S, Cerqueira MH, Gonçalves MG, Matos TT da S, Pantano G, Schultz J, Andrade JB de, Mangrich AS. 2021. Upgrading from batch to continuous flow process for the pyrolysis of sugarcane bagasse: Structural characterization of the biochars produced. J Environ Manage. 285:112145. doi:10.1016/j.jenvman.2021.112145.

Xu N, Tan G, Wang H, Gai X. 2016. Effect of biochar additions to soil on nitrogen leaching, microbial biomass and bacterial community structure. Eur J Soil Biol. 74:1–8. doi:10.1016/j.ejsobi.2016.02.004.

Yaashikaa PR, Kumar PS, Varjani S, Saravanan A. 2020. A critical review on the biochar production techniques, characterization, stability and applications for circular bioeconomy. Biotechnol Rep. 28:e00570. doi:10.1016/j.btre.2020.e00570.

Yao Y, Gao B, Inyang M, Zimmerman AR, Cao X, Pullammanappallil P, Yang L. 2011. Removal of phosphate from aqueous solution by biochar derived from anaerobically digested sugar beet tailings. J Hazard Mater. 190(1–3):501–507. doi:10.1016/j.jhazmat.2011.03.083.

Zhang L, Seagren EA, Davis AP, Karns JS. 2010. The Capture and Destruction of Escherichia coli from Simulated Urban Runoff Using Conventional Bioretention Media and Iron Oxide-coated Sand. Water Environ Res. 82(8):701–714.

Zhang W, Brown GO, Storm DE, Zhang H. 2008. Fly-Ash-Amended Sand as Filter Media in Bioretention Cells to Improve Phosphorus Removal. Water Environ Res. 80(6):507–516. doi:10.2175/106143008X266823.

Appendix

Media Characterization

2021 filter media properties are shown in Table 9. The bulk density and porosity are an average of 3 measurements, the 3 deep cores as the shallow core measurements were not accurately recorded. The moisture content is presented without standard deviation as it was only measured for the shallow cores. The infiltration data is not presented with a standard deviation as only 2 measurements were taken for each filter.

Table 9. 2021 Measured Filter Media Properties

	Sand	Biochar	IES
Bulk Density (mg/L)	1.63 ± 0.03	1.41 ± 0.06	1.63 ± 0.02
Porosity	0.34 ± 0.04	0.39 ± 0.01	0.34 ± 0.02
Moisture Content	5.6%	15.0%	4.6%
Infiltration Ksat (mm/hr)	898	1016	1418

The 2022 filter media properties are presented in Table 10. The bulk density, porosity, and moisture content are an average of 5 measurements, 3 deep cores and 2 shallow cores. The infiltration data is an average of 3 measurements.

Table 10. 2022 Measured Filter Media Properties

	Sand	Biochar	IES
Bulk Density (mg/L)	1.53 ± 0.07	1.23 ± 0.15	1.60 ± 0.08
Porosity	0.37 ± 0.07	0.43 ± 0.13	0.38 ± 0.06
Moisture Content	2.7% ± 0.01	9.8% ± 0.01	3.5% ± 0.01
Infiltration Ksat (mm/hr)	718 ± 89	1002 ± 146	969 ± 38

Table 11 shows the mineral composition of the sand used in the filter testbeds. Data was received from Plaisted Companies.

Table 11. Mineral Composition of Concrete Sand from X-ray Diffraction

Mineral	Weight percent
Quartz	65.7
K-feldspar	9.8
Plagioclase	17.6
Calcite	1.3
Dolomite	1.1
Pyrite	0.2
Total Clay Minerals (Includes illite, mica, kaolinite, and chlorite)	4.3

Figures 9 through 12 are cumulative PSD curves used in the determination of the pore size distribution of the red pine biochar and the commercial biochar, ABC Char obtained from the American Biochar Company.

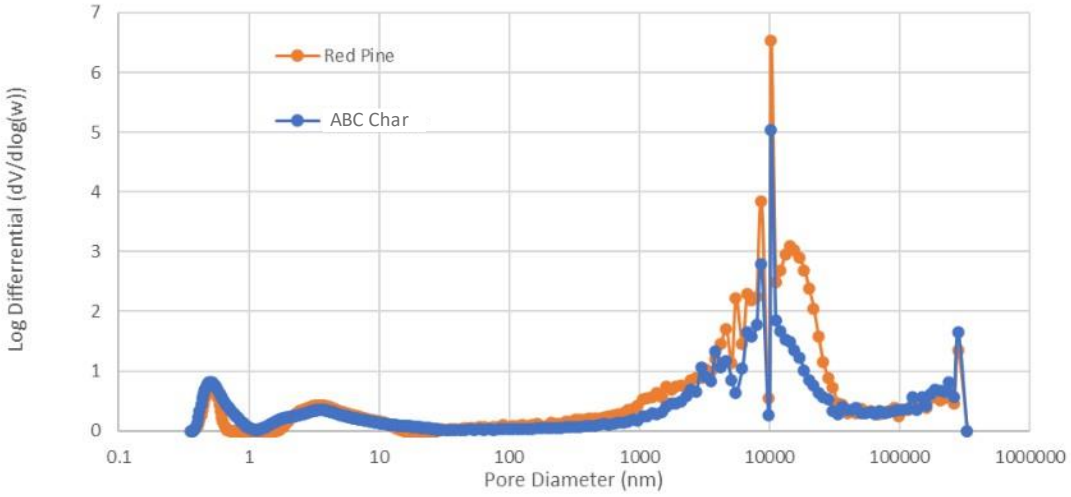

Figure 9. Differential Pore Size Distribution of Red Pine Biochar Produced at 550°C and ABC Char (0.36 nm – 1.0E6 nm)

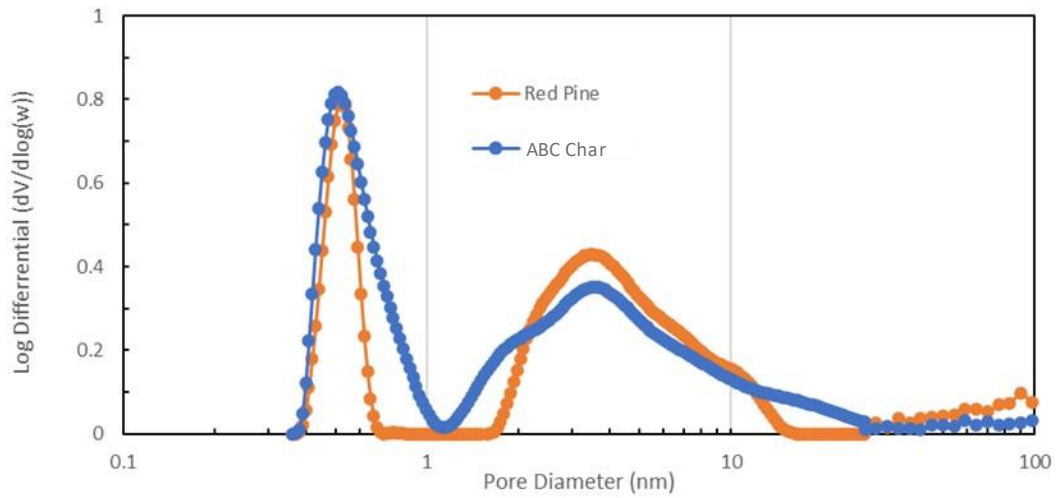

Figure 10. Differential Pore Size Distribution of Red Pine Biochar Produced at 550°C and ABC Char (0.36 nm – 100 nm)

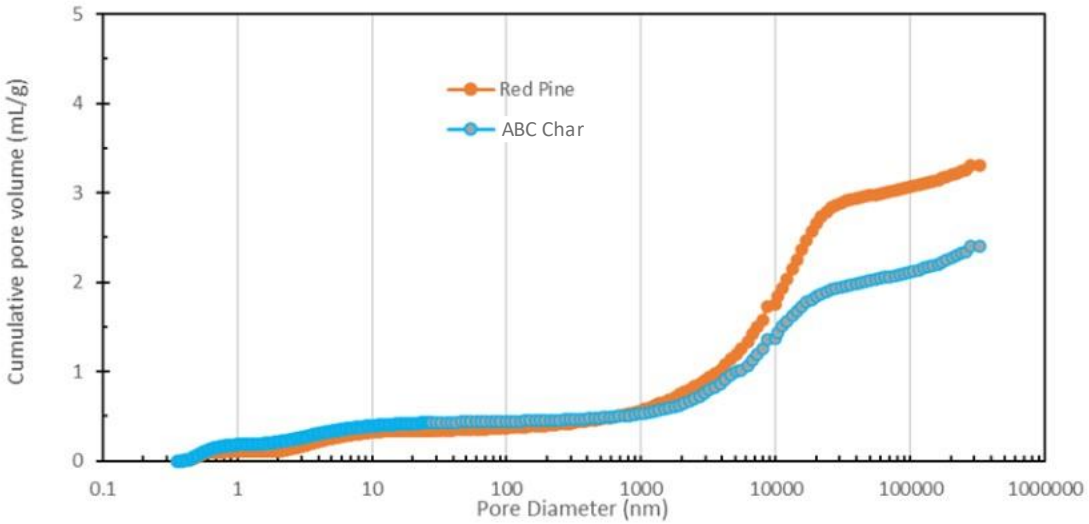

Figure 11. Cumulative Pore Volume Distribution of Red Pine Biochar Produced at 550°C and ABC Char (0.36 – 1.0E6 nm)

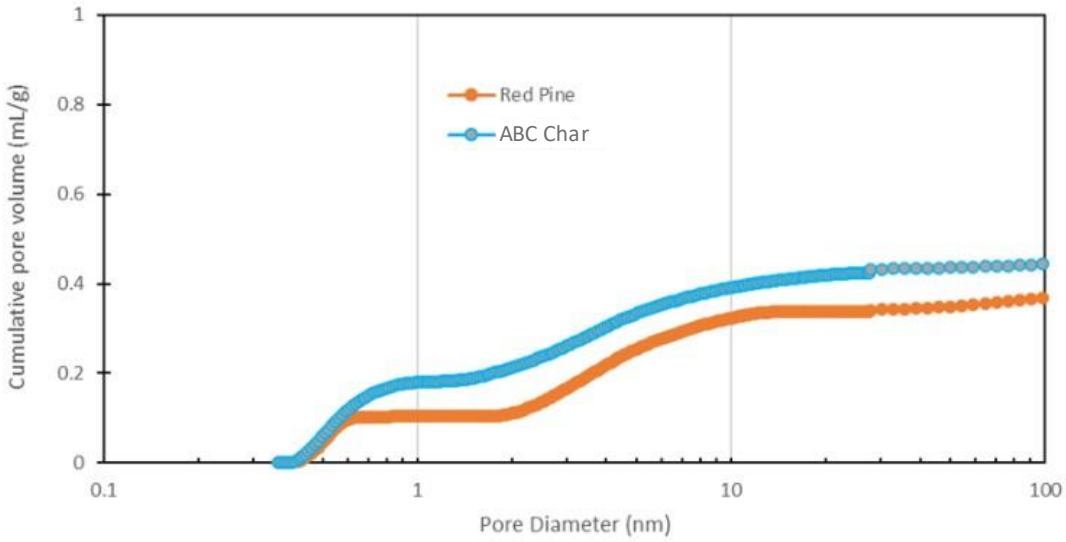

Figure 12. Cumulative Pore Volume distribution of Red Pine Biochar Produced at 550°C and ABC Char (0.36 – 100 nm)

Hydrologic Characterization

Full discharge and precipitation data for 2021 and 2022 is available as an electronic supplement.

Table 12 and 13 show the monthly cumulative discharge from the influent and effluent weir boxes for 2021 and 2022. Table 14 shows the cumulative influent and effluent discharges and precipitation for 2021 and 2022 sampling events. In 2021 the measured biochar effluent was nearly equal to the influent. Summed with the remaining measured effluent, system outflow is nearly double that of the inflow. As this is a physical impossibility, further investigation was conducted. To determine if 2021 volume balance error is caused by the influent flow sensor, the total influent volume was compared to the total runoff for each year. As seen in Table 14, the runoff and inflow values are similar. This indicates that an issue is more likely to have occurred in the effluent sensors. Sensors are initially calibrated in the factory and only recalibrated if sent back when error messages are received. No error messages were received in 2021. Therefore, flow values for the 2021 field season cannot be assumed accurate. Sensors for flow calculations were replaced before the 2022 field season. As the inflow is similar to the estimated runoff volume and the outflow is not greater than the inflow, flow data from 2022 is validated.

Table 12. Monthly Summation of 2021 Discharge (m^3)

	Sand	Biochar	IES	Parking Lot
May	17.2	15.7	12.8	22.1
June	23.4	9.0	4.5	10.2
July	38.8	18.9	11.5	43.3
August	103.6	40.4	30.4	151.5
September	44.1	14.4	13.2	32.1
October	21.5	5.4	6.7	9.5

Table 13. Monthly Summation of 2021 Discharge (m^3)

	Sand	Biochar	IES	Parking Lot
April	5.4	6.4	0.0	--
May	13.9	18.8	4.2	56.0
June	6.6	7.6	4.0	10.7
July	6.1	10.4	0.9	19.8
August	37.6	37.5	7.6	143.3
September	--	--	--	3.2

Table 14. Total Flow Through the System (m^3)

2021	
Runoff	226.18
Influent	269.93
Sand	78.92
Biochar	248.63
IES	103.85
2022	
Runoff	192.31
Influent	229.87
Sand	69.69
Biochar	80.75
IES	16.74

Table 15 shows displays a full list of characteristics for the 2022 flow equalized events.

Table 15. Full Characteristics of 2022 Flow Equalized Events

Date	20-Apr	30-Apr	19-May	15-Jun	12-Aug	17-Aug
Time Since Peak Inflow	--	--	0	15min	1hr 55min	1 min
Antecedent Dry Period	1 day	1hr 40min	18hr 50min	1 day	4 days	5 days
Antecedent Precipitation Depth (cm)	0.01	0.25	0.21	0.18	1.86	2.67
Antecedent Precipitation Volume (m3)	0.15	3.79	3.14	2.73	27.81	39.89
Precipitation Depth (cm)	1.41	2.09	0.75	0.42	2.67	0.19
Precipitation Volume (m3)	21.06	31.18	11.21	6.33	39.89	2.88
Event Measured Influent (m3)	--	--	9.11	3.44	31.47	0.45
Event Measured Sand Outflow (L)	1.05	4.08	0.99	2.05	6.34	0.30
# of Sand Pore Volumes per Event	15.8	23.4	6.8	2.6	23.6	0.3
Event Measured Biochar Outflow (m3)	1.76	4.86	1.67	1.69	6.29	0.69
# of Biochar Pore Volumes per Event	12.9	19.1	5.6	2.1	19.3	0.3
Total Event Outflow/Precipitation Volume	13%	29%	27%	81%	36%	39%

*Number of Pore volumes per event was calculated by dividing measured influent by the bed pore volume. For events without influent measurements, the precipitation volume was used.

Contaminant Concentrations

To determine any significant differences between the sand and biochar filter performances, a Pearson's p analysis was conducted. P-values for the normalized effluent concentrations are shown in table 17.

Table 16. Pearson's p Analysis for Normalized Effluent Concentrations

Contaminant	Sand vs Biochar p-value
E. coli	0.7942
TP	0.9307
Ortho P	0.8089
Nitrate	0.4627
Nickel	0.8702
Copper	0.9960
Zinc	0.4868
TOC	0.8995
TSS	0.6911

The remaining tables contain the contaminant concentrations for all contaminants measured in 2021 and 2022. Values highlighted in blue indicate values below the method detection limit. Values highlighted in green indicate approximate values.

2021 and 2022 *E. coli* concentrations are presented below in MPN/100mL.

Table 17. 2021 *E. coli* Concentrations

	Parking Lot	Sand	Biochar	IES
20-May	36400	1000	12200	7500
20-Jun	45500	6300	6300	2420
28-Jun	13500	816	8600	32
6-Jul	3100	5	308	205
14-Jul	1733	1	105	261
7-Aug	--	--	--	--
22-Aug	1553	--	--	--
24-Aug	613	201	1110	76
26-Aug	238	74	1733	77
26-Aug	248	44	249	111
8-Sep	36	1	1	1

20-Sep	96	1	1	1
20-Oct	214	1	1	1
28-Oct	17	10	8	4

Table 18. 2022 E. coli Concentrations

	Parking Lot	Sand	Biochar	IES
22-Mar	1	1	2	--
20-Apr	3	5	5	2
30-Apr	--	--	--	--
19-May	1553	291	147	72
25-May	--	--	--	--
13-Jun	1046	270	457	1
15-Jun	38300	13500	14800	20
23-Jul	238	47	816	7
26-Jul	3100	88	2420	127
6-Aug	2420	--	16	12
12-Aug	539	46	20	16
17-Aug	63	1	44	31

2021 and 2022 concentrations for trace metal sampled throughout both years are presented below as ug/L.

Table 19. 2021 Cadmium Concentrations

	Parking Lot	Sand	Biochar	IES
20-May	0.10	0.10	0.10	0.10
20-Jun	0.17	0.11	0.13	0.10
28-Jun	0.13	0.10	0.16	0.10
6-Jul	0.26	0.13	0.10	0.10
14-Jul	0.14	0.10	0.10	0.10
7-Aug	0.10	0.10	0.10	0.10
22-Aug	0.10	--	--	--
24-Aug	0.10	0.10	0.10	0.10
26-Aug	0.10	0.10	0.10	0.10
26-Aug	0.10	0.10	0.10	0.10
8-Sep	0.2	0.10	0.10	0.10
20-Sep	0.12	0.10	0.10	0.10
20-Oct	0.38	0.10	0.10	0.10
28-Oct	0.10	0.10	0.10	0.10

Table 20. 2022 Cadmium Concentrations

2022 Cadmium (ug/L)				
	Parking Lot	Sand	Biochar	IES
22-Mar	0.15	0.1	0.1	--
20-Apr	0.11	0.1	0.1	0.1
30-Apr	0.1	0.1	0.1	0.1
19-May	0.14	0.1	0.1	0.1
25-May	0.1	0.1	0.1	0.1
13-Jun	0.17	0.1	0.21	0.1
15-Jun	0.36	0.12	--	0.1
23-Jul	0.23	0.1	0.1	0.1
26-Jul	0.1	0.1	0.1	0.1
6-Aug	0.1	--	0.1	0.1
12-Aug	0.1	0.1	0.1	0.1
17-Aug	0.1	0.1	0.1	0.1

Table 21. 2021 Chromium Concentrations

	Parking Lot	Sand	Biochar	IES
20-May	1	1.7	1.1	1
20-Jun	1.6	1.9	2.1	1
28-Jun	2.8	1	1.6	1
6-Jul	4.1	1	1	1
14-Jul	3.4	1	1	1
7-Aug	1	1	1	1
22-Aug	1.6	--	--	--
24-Aug	1	1.7	1	1
26-Aug	1	1	1	1
26-Aug	1	1	1	1
8-Sep	2.4	1	1	1
20-Sep	2.1	1	1	1
20-Oct	4.8	1	1	1
28-Oct	1	1	1	1

Table 22. 2022 Chromium Concentrations

	Parking Lot	Sand	Biochar	IES
22-Mar	3.6	1.7	1.5	--

20-Apr	1.9	1.0	1.0	1.0
30-Apr	1.4	1.0	1.0	1.0
19-May	3.2	1.0	1.0	1.0
25-May	1.0	1.0	1.0	1.0
13-Jun	2.2	1.0	1.0	1.0
15-Jun	7.5	1.0	--	1.0
23-Jul	5.2	1.0	1.0	1.0
26-Jul	2.4	1.0	1.0	1.0
6-Aug	1.0	--	1.0	1.0
12-Aug	1.0	1.0	1.0	1.0
17-Aug	1.3	1.0	1.0	1.0

Table 23. 2021 Copper Concentration

	Parking Lot	Sand	Biochar	IES
20-May	7.5	14	13.4	5.2
20-Jun	15.2	45	50.9	23.2
28-Jun	18.5	19.4	14.7	12.6
6-Jul	25.2	13.8	12.4	6.3
14-Jul	12.4	6.6	6	3.4
7-Aug	4	10.6	8.2	2.1
22-Aug	9.6	--	--	--
24-Aug	4.1	10	6.1	2.3
26-Aug	7.2	5.6	3.6	2
26-Aug	2.3	4.5	3.6	1
8-Sep	89.5	4.9	4.8	1.2
20-Sep	12.4	5.2	4.6	1.1
20-Oct	34.7	6.4	6.4	2.2
28-Oct	2.5	4.1	3.8	1.6

Table 24. 2022 Copper Concentrations

2022 Copper (ug/L)				
	Parking Lot	Sand	Biochar	IES
22-Mar	10	11.4	8.6	--
20-Apr	12.5	7.4	6.2	3.5
30-Apr	7.9	4.8	3.3	0.71
19-May	11.8	7.8	4.6	1.7
25-May	3.5	4.1	7.3	1.4
13-Jun	27.4	8.8	21.1	2.3

15-Jun	41	15.4	--	7.8
23-Jul	20	8.9	3.9	3.3
26-Jul	11.5	6.1	4.6	2.5
6-Aug	7.3	--	4.4	2.2
12-Aug	2.5	2.5	3.2	0.83
17-Aug	10.5	2.6	3.3	1.2

Table 25. 2021 Lead Concentrations

	Parking Lot	Sand	Biochar	IES
20-May	1.2	1.1	0.55	1.3
20-Jun	1.5	0.64	1.4	0.5
28-Jun	2.2	0.5	1.6	0.5
6-Jul	3.6	2.3	1.4	0.74
14-Jul	2.6	0.5	0.89	0.5
7-Aug	1.1	0.84	0.64	0.57
22-Aug	1.8	--	--	--
24-Aug	1.1	1.2	0.65	0.5
26-Aug	2.1	0.5	0.5	0.5
26-Aug	0.64	0.5	0.5	0.5
8-Sep	8.5	0.5	0.5	0.5
20-Sep	4.8	0.5	0.5	0.5
20-Oct	12.8	0.5	0.5	0.57
28-Oct	0.58	0.5	0.5	0.5

Table 26. 2022 Lead Concentrations

	Parking Lot	Sand	Biochar	IES
22-Mar	6.7	2.4	1.8	--
20-Apr	3.5	0.5	0.5	1
30-Apr	3	0.67	0.5	0.71
19-May	15.2	0.5	0.5	0.5
25-May	0.96	0.5	0.5	0.5
13-Jun	1.3	0.5	0.5	0.5
15-Jun	15.3	0.52	--	0.50
23-Jul	14.6	0.50	0.50	0.50
26-Jul	4	0.50	0.50	0.50
6-Aug	1.4	--	0.50	0.50
12-Aug	0.72	0.50	0.50	0.50
17-Aug	1.5	0.50	0.50	0.50

Table 27. 2021 Nickel Concentrations

	Parking Lot	Sand	Biochar	IES
20-May	1.70	3.90	4.30	5.60
20-Jun	2.80	9.20	9.90	19.00
28-Jun	5.50	11.30	10.70	16.10
6-Jul	8.40	9.80	8.00	6.30
14-Jul	5.40	6.00	5.70	5.20
7-Aug	0.85	2.70	2.10	3.20
22-Aug	4.10	--	--	--
24-Aug	0.89	3.40	1.80	2.30
26-Aug	1.10	1.40	1.20	2.40
26-Aug	0.50	1.30	0.85	0.95
8-Sep	3.20	1.00	0.72	1.10
20-Sep	3.00	1.10	0.81	1.10
20-Oct	7	1.7	1.8	2.5
28-Oct	0.55	0.73	0.64	3.1

Table 28. 2022 Nickel Concentrations

2022 Nickel (ug/L)				
	Parking Lot	Sand	Biochar	IES
22-Mar	2.9	2.2	1.8	--
20-Apr	3.7	1.3	1.1	2.3
30-Apr	1.7	0.99	0.59	0.85
19-May	2.3	3.2	4.1	4.7
25-May	0.75	0.78	1.1	1.2
13-Jun	6.4	2.9	4.9	2.3
15-Jun	9.6	6.4	--	5.7
23-Jul	4.5	1.9	2.3	2.7
26-Jul	2.9	1.8	1.5	2.3
6-Aug	0.9	--	0.76	1.5
12-Aug	0.5	0.5	0.5	0.64
17-Aug	2.2	0.51	0.83	1.3

Table 29. 2021 Zinc Concentrations

	Parking Lot	Sand	Biochar	IES
20-May	52.0	202.0	28.9	35.9

20-Jun	223.0	55.3	52.6	53.2
28-Jun	106.0	134.0	50.8	159.0
6-Jul	218.0	229.0	90.2	111.0
14-Jul	113.0	118.0	38.4	41.4
7-Aug	35.0	13.6	12.5	8.2
22-Aug	64.8	--	--	--
24-Aug	28.5	8.8	5.5	5.0
26-Aug	52.8	13.2	8.8	26.5
26-Aug	23.1	5.0	5.0	5.0
8-Sep	218.0	92.9	29.7	42.0
20-Sep	121.0	148.0	27.2	34.0
20-Oct	340	86.7	45.4	57.5
28-Oct	77.3	10.1	5.7	5

Table 30. 2022 Zinc Concentrations

	Parking Lot	Sand	Biochar	IES
22-Mar	92	26.2	41.4	--
20-Apr	101	16.2	35	154
30-Apr	66.3	19.2	7	10.1
19-May	129	95.3	73.5	50.8
25-May	36.6	5.7	7.1	5
13-Jun	240	83	135	87
15-Jun	406	139	--	210
23-Jul	193	70.3	75.7	137
26-Jul	92.3	47.5	22.1	34.2
6-Aug	47.4	--	13	12.6
12-Aug	25	5.8	5	5.7
17-Aug	65.3	42.3	22	44.2

Titanium and barium were added to the list of contaminants measured in late-2021. To reduce costs, these medals were only sampled a few times. Concentrations are presented in ug/L.

Table 31. 2021 Titanium Concentrations

	Parking Lot	Sand	Biochar	IES
20-May	--	--	--	--
20-Jun	--	--	--	--

28-Jun	--	--	--	--
6-Jul	--	--	--	--
14-Jul				
7-Aug	4.2	17.8	12.3	2.7
22-Aug	--	--	--	--
24-Aug	--	--	--	--
26-Aug	9.9	5.6	3.9	2.8
26-Aug	3.2	14.2	8.1	1.9
8-Sep	--	--	--	--
20-Sep	19.9	2.6	1.6	1
20-Oct	--	--	--	--
28-Oct	--	--	--	--

Table 32. 2022 Titanium Concentrations

	Parking Lot	Sand	Biochar	IES
22-Mar	--	--	--	--
20-Apr	--	--	--	--
30-Apr				
19-May	30.3	114	118	69.4
25-May	--	--	--	--
13-Jun	--	--	--	--
15-Jun	81.6	98.2	93.9	64.9
23-Jul	--	--	--	--
26-Jul	--	--	--	--
6-Aug	--	--	--	--
12-Aug	--	--	--	--
17-Aug	--	--	--	--

Table 33. 2021 Barium Concentrations

	Parking Lot	Sand	Biochar	IES
20-May	--	--	--	--
20-Jun	--	--	--	--
28-Jun	--	--	--	--
6-Jul	--	--	--	--
14-Jul	--	--	--	--
7-Aug	10	20	20	10
22-Aug				
24-Aug				

26-Aug	10	30	30	10
26-Aug	0	10	10	10
8-Sep	--	--	--	--
20-Sep	28.3	16.6	12.3	5.5
20-Oct	--	--	--	--
28-Oct	--	--	--	--

Table 34. 2022 Barium Concentrations

	Parking Lot	Sand	Biochar	IES
22-Mar	--	--	--	--
20-Apr	--	--	--	--
30-Apr	--	--	--	--
19-May	25.8	68.3	68.7	16
25-May	--	--	--	--
13-Jun	--	--	--	--
15-Jun	72.5	47.2	57.3	14.1
23-Jul	--	--	--	--
26-Jul	--	--	--	--
6-Aug	--	--	--	--
12-Aug	--	--	--	--
17-Aug	--	--	--	--

2021 and 2022 chloride concentrations are presented below in mg/L.

Table 35. 2021 Chloride Concentrations

	Parking Lot	Sand	Biochar	IES
20-May	5	5	5	5
20-Jun	5	5	5	5
28-Jun	9.1	5.70	9.7	5
6-Jul	12.40	9.20	7.10	5.70
14-Jul	7.2	6.2	5	5
7-Aug	5	5	5	5
22-Aug	6	--	--	--
24-Aug	5	5	5	5
26-Aug	5	5	5	5
26-Aug	5	5	5	5
8-Sep	9.8	5	5	5
20-Sep	5	5	5	5
20-Oct	10.5	5	5	5

28-Oct	5	5	5	5

Table 36. 2022 Chloride Concentrations

	Parking Lot	Sand	Biochar	IES
22-Mar	17.1	71.9	18.6	--
20-Apr	23.2	11.2	12.9	9.8
30-Apr	5.5	5	5	5
19-May	5	12.5	15.9	13.3
25-May	5	5	5	5
13-Jun	7.1	5	7	5
15-Jun	6.4	7.7	12.9	5
23-Jul	5	5	5	5
26-Jul	5	5	5	5
6-Aug	5	--	5	5
12-Aug	5	5	5	5
17-Aug	5	5	5	5

2021 and 2022 phosphorus species concentrations are presented below in mg/L. The total phosphorus measurement was included in two analysis methods. The data presented in this thesis are an average of the two total phosphorus measurements.

Table 37. 2021 Orthophosphate Concentrations

	Parking Lot	Sand	Biochar	IES
20-May	0.01	0.01	0.01	0.01
20-Jun	0.5	0.11	0.25	0.01
28-Jun	0.35	0.01	0.06	0.01
6-Jul	1.19	0.01	0.15	0.01
14-Jul	0.12	0.01	0.02	0.01
7-Aug	0.03	0.05	0.07	0.01
22-Aug	0.06	--	--	--
24-Aug	0.05	0.1	0.1	0.01
26-Aug	0.06	0.04	0.06	0.01
26-Aug	0.05	0.07	0.06	0.01
8-Sep	--	--	--	--
20-Sep	0.02	0.01	0.02	0.01
20-Oct	0.352	0.01	0.01	0.01
28-Oct	0.057	0.032	0.03	0.01

Table 38. 2022 Orthophosphate Concentrations

	Parking Lot	Sand	Biochar	IES
22-Mar	0.045	0.129	0.12	--
20-Apr	0.037	0.014	0.01	0.01
30-Apr	0.01	0.03	0.015	0.01
19-May	--	--	--	--
25-May	0.029	0.066	0.048	0.01
13-Jun	--	--	--	--
15-Jun	0.607	0.02	0.056	0.01
23-Jul	0.106	0.2	0.175	0.013
26-Jul	0.037	0.17	0.212	0.01
6-Aug	0.066	--	0.175	0.143
12-Aug	--	--	--	--
17-Aug	0.039	0.11	0.128	0.01

Table 39. 2021 Total Phosphorus Concentrations - #1

	Parking Lot	Sand	Biochar	IES
20-May	0.258	0.177	0.135	0.041
20-Jun	0.969	0.576	1.06	0.076
28-Jun	1.56	0.16	0.415	0.079
6-Jul	1.46	0.51	0.368	0.123
14-Jul	0.853	0.11	0.144	0.02
7-Aug	0.093	0.119	0.134	0.021
22-Aug	0.992	--	--	--
24-Aug	0.083	0.151	0.126	0.02
26-Aug	0.172	0.1	0.105	0.047
26-Aug	0.092	0.102	0.085	0.02
8-Sep	0.396	0.054	0.05	0.021
20-Sep	0.291	0.026	0.036	0.02
20-Oct	0.935	0.101	0.168	0.07
28-Oct	0.109	0.072	0.066	0.037

Table 40. 2022 Total Phosphorus Concentrations - #1

	Parking Lot	Sand	Biochar	IES
22-Mar	0.188	0.223	0.204	--
20-Apr	0.198	0.059	0.03	0.054

30-Apr	0.161	0.054	0.058	0.02
19-May	0.275	0.08	0.092	0.023
25-May	0.073	0.078	0.05	0.02
13-Jun	1.34	0.165	0.389	0.032
15-Jun	1.46	0.337	0.445	0.116
23-Jul	0.478	0.273	0.267	0.047
26-Jul	0.389	0.301	0.413	0.038
6-Aug	0.167	--	0.21	0.172
12-Aug	0.063	0.148	0.167	0.02
17-Aug	0.325	0.136	0.189	0.027

Table 41. 2021 Total Phosphorus Concentrations - #2

	Parking Lot	Sand	Biochar	IES
20-May	0.032	0.020	0.020	0.020
20-Jun	0.822	0.355	0.392	0.025
28-Jun	0.477	0.032	0.140	0.020
6-Jul	1.360	0.097	0.404	0.061
14-Jul	0.258	0.029	0.161	0.020
7-Aug	0.033	0.075	0.083	0.020
22-Aug	0.169	--	--	--
24-Aug	0.074	0.105	0.114	0.020
26-Aug	0.098	0.088	0.103	0.020
26-Aug	0.074	0.075	0.093	0.020
8-Sep	0.224	0.029	0.032	0.020
20-Sep	0.056	0.020	0.022	0.020
20-Oct	0.509	0.020	0.090	0.035
28-Oct	0.056	0.033	0.029	0.020

Table 42. 2022 Total Phosphorus Concentrations - #2

	Parking Lot	Sand	Biochar	IES
22-Mar	0.056	0.174	0.135	
20-Apr	0.086	0.031	0.02	0.02
30-Apr	0.02	0.022	0.02	0.02
19-May	0.094	0.057	0.027	0.02
25-May	0.065	0.054	0.055	0.02
13-Jun	0.826	0.088	0.239	0.02
15-Jun	0.764	0.181	0.142	0.02
23-Jul	0.186	0.229	0.199	0.023

26-Jul	0.099	0.203	0.247	0.02
6-Aug	0.114		0.209	0.144
12-Aug	0.038	0.123	0.129	0.02
17-Aug	0.238	0.111	0.177	0.02

Table 43. 2021 Average Total Phosphorus Concentrations

	Parking Lot	Sand	Biochar	IES
20-May	0.145	0.0985	0.0775	0.0305
20-Jun	0.8955	0.4655	0.726	0.0505
28-Jun	1.0185	0.096	0.2775	0.0495
6-Jul	1.41	0.3035	0.386	0.092
14-Jul	0.5555	0.0695	0.1525	0.02
7-Aug	0.063	0.097	0.1085	0.0205
22-Aug	0.5805	--	--	--
24-Aug	0.0785	0.128	0.12	0.02
26-Aug	0.135	0.094	0.104	0.0335
26-Aug	0.083	0.0885	0.089	0.02
8-Sep	0.31	0.0415	0.041	0.0205
20-Sep	0.1735	0.023	0.029	0.02
20-Oct	0.722	0.0605	0.129	0.0525
28-Oct	0.0825	0.0525	0.0475	0.0285

Table 44. 2022 Average Total Phosphorus Concentrations

	Parking Lot	Sand	Biochar	IES
22-Mar	0.122	0.1985	0.1695	--
20-Apr	0.142	0.045	0.025	0.037
30-Apr	0.0905	0.038	0.039	0.02
19-May	0.1845	0.0685	0.0595	0.0215
25-May	0.069	0.066	0.0525	0.02
13-Jun	1.083	0.1265	0.314	0.026
15-Jun	1.112	0.259	0.2935	0.068
23-Jul	0.332	0.251	0.233	0.035
26-Jul	0.244	0.252	0.33	0.029
6-Aug	0.1405	--	0.2095	0.158
12-Aug	0.0505	0.1355	0.148	0.02
17-Aug	0.2815	0.1235	0.183	0.0235

2021 and 2022 concentrations for nitrogen species are presented below as mg/L.

Table 45. 2021 Ammonia Nitrogen Concentrations

	Parking Lot	Sand	Biochar	IES
20-May	0.06	0.06	0.06	0.06
20-Jun	0.44	0.06	0.07	1.01
28-Jun	1.12	0.06	0.06	0.06
6-Jul	4.22	0.06	0.51	0.15
14-Jul	1.59	0.07	0.24	0.08
7-Aug	0.06	0.06	0.06	0.13
22-Aug	1.94	--	--	--
24-Aug	0.21	0.08	0.07	0.13
26-Aug	0.7	0.06	0.06	0.06
26-Aug	0.34	0.06	0.06	0.06
8-Sep	0.83	0.06	0.06	0.06
20-Sep	0.35	0.06	0.06	0.06
20-Oct	1	0.06	0.06	0.06
28-Oct	0.09	0.06	0.06	0.06

Table 46. 2022 Ammonia Nitrogen Concentrations

	Parking Lot	Sand	Biochar	IES
22-Mar	0.22	0.1	0.07	--
20-Apr	3.02	0.07	0.13	0.4
30-Apr	0.62	0.06	0.06	0.56
19-May	1.2	0.06	0.14	0.35
25-May	0.14	0.1	0.08	0.16
13-Jun	1.77	0.45	0.33	0.06
15-Jun	1.84	0.06	0.06	0.06
23-Jul	0.65	0.09	0.52	0.06
26-Jul	0.74	0.14	0.25	0.25
6-Aug	0.06	--	0.08	0.11
12-Aug	0.31	0.06	0.06	0.08
17-Aug	0.83	0.09	0.14	0.1

Table 47. 2021 Nitrate Concentrations as N

	Parking Lot	Sand	Biochar	IES
20-May	0.2	0.52	0.2	0.38
20-Jun	0.74	1.46	0.66	0.72

28-Jun	0.20	0.81	0.20	0.20
6-Jul	0.58	0.20	0.51	0.38
14-Jul	0.20	0.20	0.45	0.64
7-Aug	0.23	0.43	0.31	0.33
22-Aug	0.20	--	--	--
24-Aug	0.20	0.36	0.36	0.33
26-Aug	0.69	1.31	0.34	0.67
26-Aug	0.29	0.24	0.26	0.25
8-Sep	0.47	0.20	0.20	0.31
20-Sep	0.58	0.21	0.20	0.20
20-Oct	1.25	0.82	0.26	0.20
28-Oct	0.20	0.20	0.20	0.20

Table 48. 2022 Nitrate Concentrations as N

	Parking Lot	Sand	Biochar	IES
22-Mar	0.2	0.38	0.27	--
20-Apr	2.19	1.26	0.72	0.24
30-Apr	0.48	0.32	0.41	0.21
19-May	0.59	2.15	0.2	0.58
25-May	0.2	0.72	0.35	0.5
13-Jun	0.32	3.85	1.26	0.39
15-Jun	0.2	2.92	0.28	0.52
23-Jul	0.89	6.5	3.08	4.34
26-Jul	0.8	2.02	2.02	2.7
6-Aug	0.4	--	0.74	0.81
12-Aug	0.2	0.25	0.74	0.32
17-Aug	0.52	0.65	2.25	1.72

Table 49. 2021 Nitrate Concentrations as N

	Parking Lot	Sand	Biochar	IES
20-May	0.06	0.06	0.06	0.06
20-Jun	0.06	0.06	0.06	0.06
28-Jun	0.20	0.06	0.06	0.06
6-Jul	0.11	0.06	0.06	0.06
14-Jul	0.21	0.06	0.06	0.06
7-Aug	0.06	0.07	0.07	0.06
22-Aug	0.06	--	--	--
24-Aug	0.06	0.06	0.06	0.06

26-Aug	0.06	0.06	0.06	0.06
26-Aug	0.06	0.06	0.06	0.06
8-Sep	0.06	0.06	0.06	0.06
20-Sep	0.07	0.06	0.06	0.06
20-Oct	0.06	0.06	0.06	0.06
28-Oct	0.06	0.06	0.06	0.06

Table 50. 2022 Nitrite Concentrations as N

2022 Nitrite N (mg/L)				
	Parking Lot	Sand	Biochar	IES
22-Mar	0.06	0.06	0.06	--
20-Apr	0.1	0.07	0.07	0.06
30-Apr	0.06	0.06	0.06	0.06
19-May	0.06	0.06	0.06	0.3
25-May	0.06	0.06	0.06	0.06
13-Jun	0.11	0.06	0.15	0.06
15-Jun	0.3	0.08	1.79	0.2
23-Jul	0.08	0.12	0.14	0.06
26-Jul	0.06	0.06	0.06	0.06
6-Aug	0.06	--	0.06	0.06
12-Aug	0.06	0.06	0.06	0.06
17-Aug	0.1	0.06	0.06	0.06

Table 51. 2021 Total Kjeldahl Nitrogen Concentrations

	Parking Lot	Sand	Biochar	IES
20-May	1.8	1.1	1.1	0.96
20-Jun	4.4	4	4.2	3.8
28-Jun	9.7	2.30	2.6	1.30
6-Jul	9.2	3.80	2.6	1.7
14-Jul	5.2	1.5	1.4	1.2
7-Aug	0.72	0.73	0.75	0.68
22-Aug	8.9	--	--	--
24-Aug	0.56	0.38	0.36	0.32
26-Aug	1.6	0.65	0.43	0.55
26-Aug	1	0.24	0.18	0.18
8-Sep	3.9	0.4	0.44	0.43
20-Sep	3.4	0.61	0.55	0.5
20-Oct	5.5	1	0.86	0.85

28-Oct	0.47	0.25	0.27	0.26

Table 52. 2022 Total Kjeldahl Nitrogen Concentrations

	Parking Lot	Sand	Biochar	IES
22-Mar	1	0.94	0.64	--
20-Apr	6.4	1.3	1.2	0.97
30-Apr	2	0.32	0.22	0.82
19-May	2.6	0.84	0.7	0.83
25-May	0.61	0.4	0.3	0.37
13-Jun	7.3	1.8	2.6	0.68
15-Jun	7.2	2.3	3.3	0.87
23-Jul	3.9	1.3	1.4	0.75
26-Jul	3	1.2	1.1	1
6-Aug	0.94	--	0.76	0.69
12-Aug	0.66	0.26	0.21	0.23
17-Aug	3.7	0.32	1.2	0.49

2021 and 2022 hardness concentrations are presented below as mg/L $CaCO_3$.

Table 53. 2021 Hardness Concentrations

	Parking Lot	Sand	Biochar	IES
20-May	45	59	47	45
20-Jun	45	80	75	80
28-Jun	45	120	105	82
6-Jul	96	140	116	59
14-Jul	70	98	88	59
7-Aug	45	45	45	45
22-Aug	63	--	--	--
24-Aug	45	45	45	45
26-Aug	45	45	51	45
26-Aug	45	45	45	45
8-Sep	45	45	45	45
20-Sep	45	47	45	45
20-Oct	45	67	68	56
28-Oct	45	45	45	45

Table 54. 2022 Hardness Concentrations

	Parking Lot	Sand	Biochar	IES
22-Mar	45	45	45	--
20-Apr	45	45	45	45
30-Apr	45	45	45	45
19-May	45	161	45	102
25-May	45	45	45	45
13-Jun	56	97	85	61
15-Jun	67	151	132	94
23-Jul	45	97	110	76
26-Jul	45	78	64	69
6-Aug	45	--	--	45
12-Aug	45	45	45	45
17-Aug	45	45	49	53

2021 and 2022 total organic carbon concentrations are presented below as mg/L.

Table 55. 2021 Total Organic Carbon Concentrations

	Parking Lot	Sand	Biochar	IES
20-May	20.5	17	20.9	23.2
20-Jun	32	76.4	86.4	77.6
28-Jun	106	43.2	66.8	32.4
6-Jul	149	39.6	41.6	33.3
14-Jul	66.3	41.4	30.6	28.8
7-Aug	10.6	12.4	12.2	10.1
22-Aug	54.4	--	--	--
24-Aug	8.5	8.1	6.7	5.6
26-Aug	12.8	11	8.3	9.7
26-Aug	6.7	3.1	3	2.7
8-Sep	47.2	3.4	4.4	4.3
20-Sep	31.1	7.7	6.3	5.5
20-Oct	95.1	10.6	13.2	10
28-Oct	17.2	7.6	11.2	9.7

Table 56. 2022 Total Organic Carbon Concentrations

	Parking Lot	Sand	Biochar	IES
22-Mar	6.3	7.8	6.9	--
20-Apr	41.9	14	13.3	5.6

30-Apr	11.7	2.7	2.4	2.4
19-May	10.4	14.3	12.6	10.4
25-May	10.3	7	7.2	5
13-Jun	101	18.5	51.3	9.2
15-Jun	74.4	34.6	38.4	14.2
23-Jul	29.6	10	9.3	6
26-Jul	29.2	14.2	13.1	8.4
6-Aug	8.8	--	9.8	7.8
12-Aug	--	--	--	--
17-Aug	27.2	2.9	12.2	4.1

2021 and 2022 concentrations for conductivity and specific conductivity are presented below as uS/cm.

Table 57. 2021 Conductivity Concentrations

	Parking Lot	Sand	Biochar	IES
20-May	50.9	135.6	115.2	87.5
20-Jun	133.4	181.4	203.9	184.7
28-Jun	215.7	304.90	357.20	196.80
6-Jul	327.60	337.80	340.5	212.3
14-Jul	248	288.1	270.7	204.9
7-Aug	34.3	78.9	89.4	76.3
22-Aug	161.3	--	--	--
24-Aug	26.8	60.3	65.3	65.4
26-Aug	35.8	138.5	146.8	98.6
26-Aug	24	44.8	48.5	56.1
8-Sep	104.3	74.4	65.3	78.1
20-Sep	90.8	102.6	92.4	76.2
20-Oct	138.9	160.9	148.6	128.5
28-Oct	40.3	70.7	58.8	64.4

Table 58. 2022 Conductivity Concentrations

	Parking Lot	Sand	Biochar	IES
22-Mar	--	--	--	--
20-Apr	162.9	109.5	153.2	158.1
30-Apr	46.7	80.8	68.4	52.8
19-May	28.1	321	380.7	375.5
25-May	29	77.5	74.2	75.6

13-Jun	213.9	168.3	216.8	233
15-Jun	18.6	231.2	332.6	311.5
23-Jul	78.9	230.1	302.9	263.5
26-Jul	96.1	218.1	213.4	212.8
6-Aug	30.1	88	47.1	40.2
12-Aug	21.7	76.5	42	--
17-Aug	--	--	--	--

Table 59. 2021 Specific Conductivity Concentrations

	Parking Lot	Sand	Biochar	IES
20-May	63.3	165.9	141.5	109.1
20-Jun	142.6	188.9	213.4	193.7
28-Jun	220	315	366	202.3
6-Jul	349	358.6	354.1	223.2
14-Jul	260.8	299.1	278.9	209.8
7-Aug	36.6	83.2	95	80.5
22-Aug	177.3	--	--	--
24-Aug	29.1	64.6	70.2	69.9
26-Aug	39.1	147.2	157.5	105.7
26-Aug	26.4	49.6	53.7	62
8-Sep	111.9	80.8	70.9	83.8
20-Sep	96.8	110.2	99.3	81.6
20-Oct	175.1	209.3	195.9	168.4
28-Oct	57.6	100.6	84.6	91.9

Table 60. 2022 Specific Conductivity Concentrations

	Parking Lot	Sand	Biochar	IES
22-Mar				
20-Apr	248.6	173.8	244.5	245.5
30-Apr	64.6	113.5	95.9	74.9
19-May	33.3	370	118.6	440.1
25-May	37.6	98.1	93.6	95.9
13-Jun	237.1	182.5	238.6	254.8
15-Jun	198	245.8	353.4	334.9
23-Jul	80.4	234.7	296	265.5
26-Jul	100.2	225.3	217.3	218.2
6-Aug	41	120.4	79.1	45.4
12-Aug	24.5	85.5	47.5	--

17-Aug	--	--	--	--

The 2021 and 2022 salinity concentrations are presented below as ppt.

Table 61. 2021 Salinity Concentrations

	Parking Lot	Sand	Biochar	IES
20-May	0.03	0.08	0.07	0.05
20-Jun	0.07	0.09	0.1	0.09
28-Jun	0.1	0.15	0.17	0.1
6-Jul	0.17	0.17	0.17	0.11
14-Jul	0.12	0.14	0.13	0.1
7-Aug	0.02	0.04	0.04	0.04
22-Aug	0.08	--	--	--
24-Aug	0.01	0.03	0.03	0.03
26-Aug	0.02	0.07	0.07	0.05
26-Aug	0.01	0.02	0.02	0.03
8-Sep	0.05	0.04	0.03	0.04
20-Sep	0.04	0.05	0.05	0.04
20-Oct	0.08	0.1	0.09	0.08
28-Oct	0.03	0.05	0.04	0.04

Table 62. 2022 Salinity Concentrations

	Parking Lot	Sand	Biochar	IES
22-Mar	--	--	--	--
20-Apr	0.12	0.08	0.12	0.12
30-Apr	0.03	0.05	0.04	0.03
19-May	0.01	0.18	0.22	0.21
25-May	0.02	0.05	0.04	0.04
13-Jun	0.11	0.09	0.11	0.23
15-Jun	0.09	0.12	0.17	0.16
23-Jul	0.04	0.11	0.14	0.13
26-Jul	0.05	0.11	0.1	0.1
6-Aug	0.02	0.06	0.04	0.02
12-Aug	0.01	0.04	0.02	--
17-Aug	--	--	--	--

2021 and 2022 solids and transparency data are presented below. Solids data is presented as mg/L and transparency as 1/100cm.

Table 63. 2021 Total Suspended Solids Concentrations

	Parking Lot	Sand	Biochar	IES
20-May	16	28	12	6
20-Jun	26	30	41	5
28-Jun	57	18	24	6
6-Jul	57	34	11	14
14-Jul	50	4	6	6
7-Aug	11	15	11	3
22-Aug	58	--	--	--
24-Aug	14	13	8	3
26-Aug	28	5	2	3
26-Aug	7	9	4	2
8-Sep	37	8	7	6
20-Sep	59	5	3	4
20-Oct	124	10	7	12
28-Oct	4	2	1	1

Table 64. 2022 Total Suspended Solids Concentrations

	Parking Lot	Sand	Biochar	IES
22-Mar	54	17	16	--
20-Apr	31	4	4	9
30-Apr	28	9	3	3
19-May	80	5	4	4
25-May	10	3	3	3
13-Jun	24	8	8	3
15-Jun	179	15	13	4
23-Jul	134	3	4	4
26-Jul	35	3	3	3
6-Aug	13	--	3	3
12-Aug	6	3	3	3
17-Aug	19	3	3	3

Table 65. 2021 Volatile Suspended Solids Concentrations

	Parking Lot	Sand	Biochar	IES
20-May	15	13	6	5

20-Jun	24	19	22	4
28-Jun	29	17	12	6
6-Jul	30	28	5	8
14-Jul	30	5	5	3
7-Aug	7	3	3	2
22-Aug	53	--	--	--
24-Aug	7	3	2	1
26-Aug	16	3	1	2
26-Aug	5	2	2	1
8-Sep	23	4	6	6
20-Sep	32	5	3	4
20-Oct	65	7	5	11
28-Oct	3	1	1	1

Table 66. 2022 Volatile Suspended Solids Concentrations

	Parking Lot	Sand	Biochar	IES
22-Mar	27	6	5	--
20-Apr	14	3	3	3
30-Apr	17	3	3	3
19-May	28	3	3	4
25-May	7	3	3	3
13-Jun	21	5	8	3
15-Jun	75	12	12	3
23-Jul	--	--	--	--
26-Jul	17	3	3	3
6-Aug	8	--	3	3
12-Aug	4	3	3	3
17-Aug	13	3	3	3

Table 67. 2021 Transparency Measurements

	Parking Lot	Sand	Biochar	IES
20-May	--	--	--	--
20-Jun	38.5	29	32	82
28-Jun	14	39.5	28.5	57
6-Jul	--	--	--	--
14-Jul	11.5	100	73.5	71.5
7-Aug	45.5	26	34.5	89.5
22-Aug	25	--	--	--

24-Aug	--	--	--	--
26-Aug	--	--	--	--
26-Aug	40	35	40	51
8-Sep	20	100	100	100
20-Sep	--	--	--	--
20-Oct	9	90	100	100
28-Oct	--	--	--	--

Table 68. 2022 Transparency Measurements

	Parking Lot	Sand	Biochar	IES
22-Mar	15	27	23	--
20-Apr	26	87	100	100
30-Apr	--	--	--	--
19-May	24	100	100	100
25-May	51	100	100	100
13-Jun	19	86	68	100
15-Jun	7	100	77	100
23-Jul	11	100	100	100
26-Jul	22	100	100	100
6-Aug	49	100	100	100
12-Aug	87	--	100	100
17-Aug	--	--	--	--

2021 and 2022 data for pH, temperature, and dissolved oxygen (DO) are presented below. Temperature data is presented as ^{o}C. The DO data is presented as mg/L.

Table 69. 2021 pH Measurements

	Parking Lot	Sand	Biochar	IES
20-May	8.3	7.7	7.4	7.7
20-Jun	7.7	8	8.3	8
28-Jun	6.5	6.4	6.4	6.4
6-Jul	6	6.2	6.4	6.6
14-Jul	6.9	7.3	7.4	7
7-Aug	7.8	7.6	8.1	8.6
22-Aug	8.6	--	--	--
24-Aug	7.6	7.7	7.6	7.6
26-Aug	8.5	7.8	7.5	7.9
26-Aug	7.7	7.8	8.1	7.8

8-Sep	7.6	7.7	7.7	8.1
20-Sep	6.6	6.7	6.9	6.5
20-Oct	7.56	8.09	7.73	7.37
28-Oct	7.91	7.77	8.05	8.53

Table 70. 2022 pH Measurements

	Parking Lot	Sand	Biochar	IES
22-Mar	--	--	--	--
20-Apr	8.6	9.58	8.86	8.73
30-Apr	8.96	9.14	8.56	8.73
19-May	8.16	7.71	7.49	7.56
25-May	9	8.33	8.2	8.14
13-Jun	6.54	6.66	6.51	7.48
15-Jun	7.84	7.92	8.04	7.74
23-Jul	9.13	8.15	8.12	8.36
26-Jul	7.54	7.15	7.14	7.05
6-Aug	7.13	7.22	6.95	8.59
12-Aug	8.81	9.17	8.85	--
17-Aug	--	--	--	--

Table 71. 2021 DO Concentrations

	Parking Lot	Sand	Biochar	IES
20-May	1.47	7.09	3.04	4.94
20-Jun	7.12	6.31	5.93	4.06
28-Jun	4.08	4.37	3.27	6.21
6-Jul	3.47	4.91	4.44	4.38
14-Jul	3.05	4.92	5.34	4.18
7-Aug	7.57	6.23	5.63	3.05
22-Aug	0.71	--	--	--
24-Aug	8.21	7.6	7.05	4.54
26-Aug	8.6	5.65	5.45	4.1
26-Aug	8.5	8.27	7.72	4.1
8-Sep	6.76	8.77	8.82	9.46
20-Sep	6.36	7.84	7.62	8.46
20-Oct	9.17	9.59	8.79	10.73
28-Oct	10.35	8	8.21	5.79

Table 72. 2022 DO Concentrations

	Parking Lot	Sand	Biochar	IES
22-Mar	--	--	--	--
20-Apr	9.26	9.5	8.95	8.63
30-Apr	9.7	5.95	8.56	9.01
19-May	8.82	4.95	4.33	5.04
25-May	9.52	4.35	6.07	7.27
13-Jun	2.82	6.84	5	6.08
15-Jun	5.93	4.64	3.12	4.91
23-Jul	8.02	4.92	4.06	5.1
26-Jul	6.11	5.12	4.33	5.06
6-Aug	7.81	8.45	8.51	8.3
12-Aug	8.98	5.52	7.72	--
17-Aug	--	--	--	--

Table 73. 2021 Water Temperature Measurements

	Parking Lot	Sand	Biochar	IES
20-May	14.8	15.4	30.3	14.56
20-Jun	21.6	22.9	22.7	22.6
28-Jun	24	23.3	23.7	23.6
6-Jul	21.8	22	23	22.4
14-Jul	22.3	23.1	23.5	23.8
7-Aug	21.7	22.3	21.9	22.3
22-Aug	20.3	--	--	--
24-Aug	20.9	21.5	21.3	21.6
26-Aug	20.5	21.9	21.4	21.5
26-Aug	20.2	20	19.9	20.1
8-Sep	21.4	20.8	20.9	21.4
20-Sep	21.8	21.4	21.4	21.6
20-Oct	14.2	12.9	12.4	12.6
28-Oct	9.3	9.5	9	9.4

Table 74. 2022 Water Temperature Measurements

	Parking Lot	Sand	Biochar	IES
22-Mar	--	--	--	--
20-Apr	6.9	5.6	5.5	6.4
30-Apr	10.5	9.9	10	9.6
19-May	16.9	18.1	17.1	17.3

25-May	13.1	14	14.2	13.9
13-Jun	19.9	20.9	20.2	20.5
15-Jun	21.5	21.9	21.9	21.3
23-Jul	24.1	24	26.2	24.6
26-Jul	22.9	23.3	24.1	23.7
6-Aug	11.1	10.9	3.8	19
12-Aug	19	19.5	19	--
17-Aug	--	--	--	--